EarthArXiv preprint

This manuscript is the revised version of the preprint uploaded to EarthArXiv in June 2020.

Round one: It has been submitted for publication to Terra Nova and was rejected.

Round two: It was submitted to Marine and Petroleum Geology in June 2020 and received major revisions in September 2020; a revised manuscript was resubmitted in December 2020.

Round three: It received moderate revisions in December 2020 and a revised manuscript was resubmitted in February 2021 (this preprint version).

This preprint version of the manuscript is undergoing peer-review and has not yet been accepted for publication.

Authors encourage downloading the latest manuscript version from EarthArXiv before usage.

Authors welcome comments, feedback and discussions anytime. Please, feel free to contact the first author at r.j.g.charton@tudelft.nl

---

Syn-depositional Mesozoic siliciclastic pathways on the Moroccan Atlantic margin linked to evaporite mobilisation

Authors

Rémi Charton,
Department of Geoscience and Engineering, Delft University of Technology,
P.O. Box 5048, 2600 GA Delft, The Netherlands
and North Africa Research Group, University of Manchester, UK.
r.j.g.charton@tudelft.nl (corresponding author)

Christian Kluge,
Helmholtz Centre Potsdam - GFZ German Research Centre for Geosciences, Telegrafenberg, 14473 Potsdam, Germany
christian.kluge@gfz-potsdam.de

David Fernández-Blanco,
Consejo Superior de Investigaciones Científicas (CSIC), Instituto de Ciencias del Mar (ICM), Passeig Marítim de la Barceloneta, 37-49, E-08003 Barcelona, Spain.
geo.david.fernandez@gmail.com

Aude Duval-Arnould,
School of Earth and Environmental Sciences, The University of Manchester, M13 9PL Manchester, United Kingdom
and North Africa Research Group, University of Manchester, UK.
aude.duval-arnould@manchester.ac.uk

Orrin Bryers
School of Earth and Environmental Sciences, The University of Manchester, M13 9PL Manchester, United Kingdom
and North Africa Research Group, University of Manchester, UK.
orrin.bryers@manchester.ac.uk

Jonathan Redfern,
School of Earth and Environmental Sciences, The University of Manchester, M13 9PL Manchester, United Kingdom
and North Africa Research Group, University of Manchester, UK.
jonathan.redfern@manchester.ac.uk

and Giovanni Bertotti,
Department of Geoscience and Engineering, Delft University of Technology,
P.O. Box 5048, 2600 GA Delft, The Netherlands
and North Africa Research Group, University of Manchester, UK.
g.bertotti@tudelft.nl

Abstract

Evaporite mobilisation in evaporite-cored anticlines leads to topographic growth that can alter sedimentary routing in shallow marine environments. This paper analyses two evaporite-cored anticlines perpendicular to the NW Africa coast to understand how their tectonic evolution influenced sediment pathways during the Early to Middle Jurassic and Early Cretaceous exhumation of the Mesozoic margin hinterland. The Essaouira-Agadir Basin in Morocco underwent evaporite deposition during the Atlasic and Atlantic rifting. Subsequent loading and tectonics resulted in re-mobilisation and generation of a variety of evaporite structures. Structural data obtained from analysis of Google Earth images processed using Move 2D allowed derivation of the thickness of sedimentary units on both flanks of the structures. Integrated with sedimentary logs from nine locations around evaporite-cored structures and two onshore wells, this data constrains the depositional record and allow an assessment of siliciclastic flux in the Essaouira-Agadir Basin. The results show the importance of syn-sedimentary evaporite tectonics on basin morphology, which influences the distribution of clastics delivered by fluvial systems and deepwater processes into the basin. This paper constrains the evolution of the Amsittène and Imouzzer anticlines in the Early to Middle Jurassic and support that their growth is associated with halokinesis. Mesozoic syn-sedimentary fold growth would have provided an important control on sediment discharge pathways and on the location of sediment entry points on the shelf margin, that ultimately fed deep water fan systems. This knowledge is key to predict the reservoir presence on the eastern margin of the Central Atlantic Ocean and to some extent, its conjugate margin in Nova Scotia.

1. Introduction

In the absence of tectonic forces, the mobility of weak evaporites could lead to surface topography influences potential sediment pathways (e.g., Venus et al., 2015). Extensive fieldwork and high-resolution 3D seismic surveys document this relationship between halokinesis and sediment channelling in fluvial and shallow-marine environments (e.g., Venus et al., 2015; Rojo and Escalona, 2018). However, this relationship is poorly documented in remote onshore areas and/or in areas with scarce field data.

Evaporite mobility markedly affected the post-rift evolution of the Moroccan passive margin, in NW Africa (e.g., Pichel et al., 2018). An outstanding example is the influence of Triassic evaporites of the Eastern Diapiric Province in the post-rift sedimentary architecture of Agadir-Essaouira Basin (EAB) in the Western High Atlas (WHA, **Fig. 1**) (e.g., Michard et al., 2008). The present-day onshore segment of the EAB is the only Atlantic coastal basin in NW Africa bearing Triassic evaporites (Hafid et al., 2008). Furthermore, thickest evaporitic bodies in the EAB platform domain, as well as their Jurassic cover, are located atop of half-grabens (Tari et al., 2003).

The intense influence of halokinesis in this basin is expressed as evaporite-cored anticlines in the onshore, allochthonous evaporite bodies, diapirs and tongues offshore Essaouira, and up-right tear-drop diapirs offshore Agadir (Hafid et al., 2008; Pichel, 2018). Towards the east, in the interior of the Africa tectonic plate, evidences along segments of the Central High Atlas suggest that the former rift basin was also intensely deformed by diapirs during the Jurassic (Saura et al., 2014; Verges et al., 2017; Moragas et al., 2018). There and in the Western High Atlas, folding of the Mesozoic platform series has historically been attributed to the recent deformations of the Atlas orogeny (Ager, 1974; Frizon de Lamotte et al., 2008).

The EAB evolution is dominated by rifting events, near complete Mesozoic sedimentation, and localised to regional erosion surfaces (Ambroggi, 1963; Ager, 1974; Ellouz et al., 2003; Michard et al., 2008; Luber, 2017). Its suspected Mesozoic hinterlands - the Meseta massif to the northeast, High Atlas Massif ancient directly adjacent to the east, and the Anti-Atlas to the south and southeast - show important variations in their exhumation and burial histories (e.g., Frizon de Lamotte et al., 2009; Domenech, 2015; Ghorbal et al., 2008; Saddiqi et al., 2009; reviewed and synthetised in Charton et al., 2020). The former basin developed at the junction

between the Central Atlantic and Atlasic riftings during the Triassic to Early Jurassic, and was exhumed during Alpine shortening (e.g., Michard et al., 2008). Presently part of the Western High Atlas after the Cenozoic Alpine-related exhumation, the basin exposes tens of km-long evaporite-cored anticlines roughly perpendicular to the coast line (Michard et al., 2008). It is unclear if Jurassic to Cretaceous km-scale exhumation events of the massifs surrounding the EAB (Charton et al., 2020) contributed to evaporite mobilisation and/or led to topographic growth of the anticlines (namely Tidsi, Amsittène, Imouzzer, Cap Rhir, Anklout, and Lgouz; **Fig. 1c**), thereby modulating former fluvial pathways delivering sediments from the Meseta, High Atlas, and Anti-Atlas domains (Luber, 2017).

This paper constrains timing and evolution of evaporite-cored anticlines in the Western High Atlas and discusses whether onshore sediment pathways and offshore sediment distribution are controlled by the topographic expression of those anticlines. We present a workflow to gather remotely geological, structural and stratigraphical data, and to derive cross-sections that are unfolded. We investigate stratigraphic variations in thicknesses, and the position and timing of the unconformities, to unravel the episodes of anticline growth, either by diapirism or by tectonic shortening (Fernández-Blanco et al., 2020). Results allow us to compare the time of evaporite mobilisation in the onshore, in the offshore and in the Central High Atlas basin, and thus, the discussion on potential links with the vertical motions across the Moroccan passive margin.

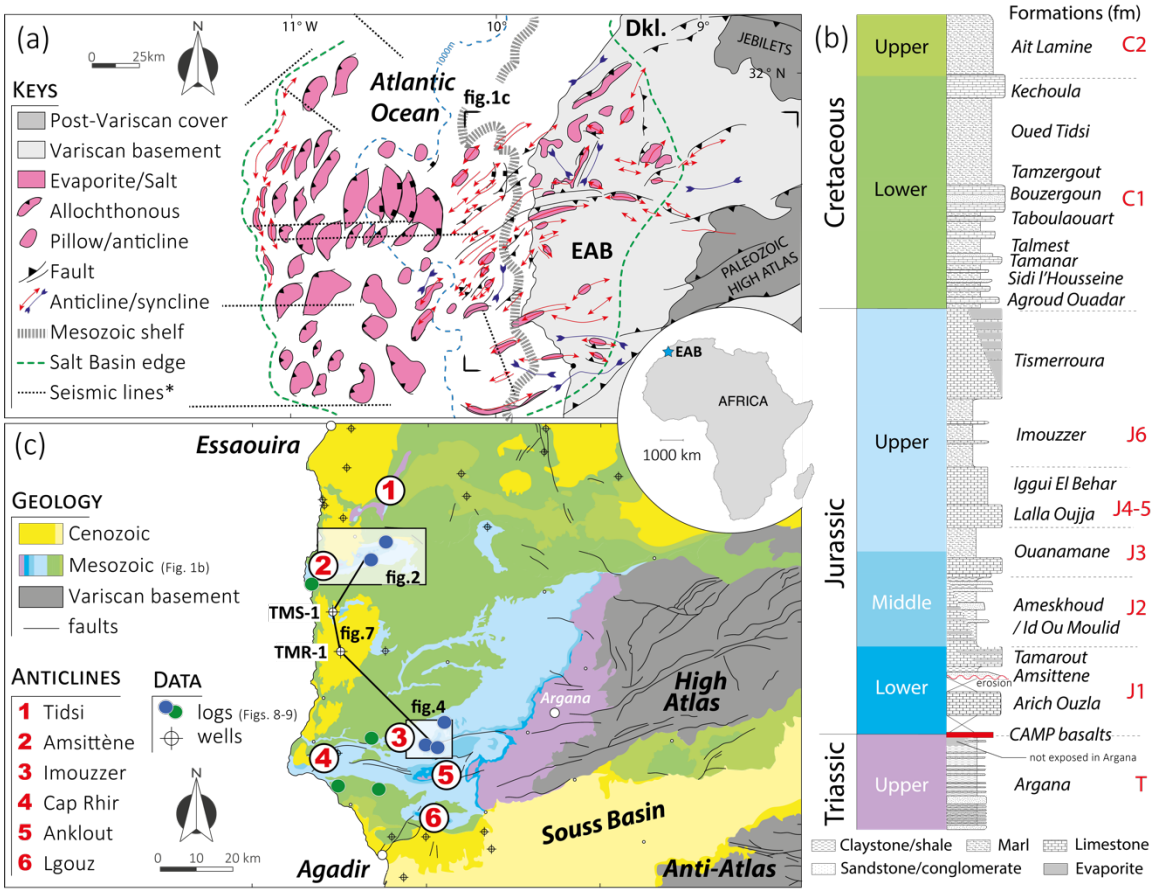

Figure 1 | a) Map of evaporite structures in the Agadir-Essaouira Basin (EAB) in relation with faults and folds (after Tari et al., 2012). *Seismic lines presented and interpreted in Pichel et al. (2019). b) Mesozoic litho-stratigraphic column (after Choubert, 1957, Michard et al., 2008; Luber, 2017; Mader et al., 2017; Duval-Arnould, 2019). Red letters alongside the formation names are the references used in the present work for the unfolding of the cross-section. c) Geological map of the area (after Hollard et al., 1985) showing the Western High Atlas anticlines (numbered 1 through 6). Names and precise location of the logs are presented in table 1.

Period	Locality/Name	Stages	Anticline	Latitude [decº]	Longitude [decº]	Elevation [m]
Jurassic (fig. 8)	Amsittene East (AME)	Callovian-Oxfordian	Amsittène	31.199	-9.595	635
	Amsittene Callovian (AMCA)	Callovian-Oxfordian	Amsittène	31.159	-9.679	807
	Assif El Hade (ASH)	Aalenian-Oxfordian	Imouzzer	30.725	-9.464	1053
	Tidili (TID)	Callovian-Oxfordian	Imouzzer	30.684	-9.500	945
	Imouzzer (IMZ)	Callovian-Oxfordian	Imouzzer	30.687	-9.478	1179
Cretaceous (fig. 9)	Ain Hammouch (AH)	Berriasian-Aptian	Cap Rhir	30.613	-9.698	203
	Igourar (IG)	Berriasian-Aptian	Cap Rhir	30.735	-9.728	138
	Sidi Bouskri (SB)	Berriasian-Valanginian	Cap Rhir	30.613	-9.769	108
	Amsittene-1 (AMS)	Hauterivian	Amsittène	31.097	-9.816	80

Table 1 | Location of the stratigraphic logs used in this work (after Duval-Arnould, 2019 and Bryers, pers comm.).

2. Geological setting

2.1. Geological history

The Western High Atlas (WHA) presently connects the High Atlas fold belt, which is an inverted Triassic-Jurassic rift basin of the Tethys, to the Atlantic passive margin (**Fig. 1**; Michard et al., 2008; Teixell et al., 2003). The Essaouira-Agadir Basin (EAB), now deformed and exposed in the WHA, was surrounded during its Mesozoic history by other coastal basins to the north and south (Doukkala and Souss Basins, respectively; **Fig. 1a**) and by a series of Variscan massifs to the northeast, east, and southeast (Meseta, Massif Ancien, and Anti-Atlas, respectively).

The Late Palaeozoic Variscan orogeny affected the Precambrian basement and its Palaeozoic marine-dominated sedimentary cover (Michard et al., 2010; Ellero et al., 2020). The chain collapsed between the Late Permian and Early Triassic (regionally called 'Hercynian' unconformity; e.g., Frizon de Lamotte et al., 2013). The pre-rift basement of the EAB was deformed by two partly-coeval rifting events, that started during the Triassic and continued into the Jurassic: The Central Atlantic rift (ca. 230-190 Ma; Labails et al., 2010) and the Atlasic-Tethysian rift (aborted; ca. 240-185 Ma; Piqué et al., 2006), at a ~45° angle to one another.

The Mesozoic sedimentary record exposed in the Western High Atlas is arguably one of the most complete and fully exposed of NW Africa (e.g., Hafid et al., 2000, Luber, 2017; Duval-Arnould, 2019). The thickness of syn- and post-rift Mesozoic sequences reaches up to c. 7 km in the EAB onshore (Ellouz et al., 2003; Zühlke et al., 2004; Tari and Jabour, 2013; Luber, 2017; Duval-Arnould, 2019). In the offshore EAB, large-scale anticlines, lacking consistent orientation as formed by salt/evaporite diapirism, are well imaged and based on mini-basin architecture, thought to have started in the Jurassic (e.g., Hafid et al., 2006; Pichel et al., 2019; **Figs. 1b** and **1c**).

The Africa-Europe collision forced the Alpine inversion since Late Cretaceous (Hafid et al., 2006; see synthesis in Frizon de Lamotte et al., 2008). N-NW/S-SE directed shortening led to the reactivation of rift-related normal faults and buckling the Mesozoic sedimentary cover, ultimately resulting in the thick-skinned thrusting and folding (Teixell et al., 2003). The Alpine compressional phase overprinted evaporite-cored anticlines, thereby hindering our capacity to infer evaporite mobility during the Mesozoic (Michard et al, 2008).

2.2. Mesozoic stratigraphy

2.2.1. Triassic

Terrestrial sediments were deposited throughout the Essaouira-Agadir Basin during Triassic rifting of the region, under dominantly arid conditions. They are exposed in the Argana Valley, where between 2500 to 5000 m thick sequence of red beds form spectacular outcrops (**Fig. 1b**) (Brown, 1980; Piqué et al., 2002, Mader and Redfern, 2011; Ellero et al., 2012). Triassic continental clastics have also been encountered in a number of wells drilled across the basin, and the rift architecture imaged on seismic data.

Facies associations recognised, representing proximal and distal facies belts in a continental rift, include ephemeral braided river systems, wet aeolian sandflats, perennial fluvial channel deposits and extensive floodplain / play lake mudrocks and evaporites (Mader and Redfern 2011; Mader et al., 2017). The evaporites are dominantly intercalated toward the top of this sequence and can reach considerable thickness, probably in excess of 1km offshore (salt, anhydrites, gypsum, and halite in onshore subsurface; Mader et al., 2017; halite and gypsum at the outcrop). In most areas, where thickly developed, they show evidence of later remobilisation due to loading, developing extensive diapiric structures and salt walls (Hafid, 2000; Hafid et al., 2006; Tari and Jabour, 2013; **Fig. 1a**). Thickness changes are attributed to the initial configuration of the rifted sub-basins, controlled by pre- and syn- rift basement architecture (Ager, 1974; Tari and Jabour, 2013; Pichel et al., 2019), with evaporite deposition controlled by syn-depositional topography, being favoured within half-grabens depocenters (Hafid et al., 2006; Perez et al., 2019). Overlying the Triassic sequence, two tholeiitic basalt flows of the Central Atlantic Magmatic Province (CAMP) yield absolute ages of ~201 Ma (i.e., Late Rhaetian; Knight et al., 2004; Michard et al., 2008).

2.2.2. Jurassic

The earliest Jurassic deposits record marine carbonates in the northern part of the study area (Jbel Amsittène and well ESS-1). These carbonates are heavily dolomitized, but part of the original fabric of the Amsittène outcrops is still preserved and contain rare ammonites, brachiopods and abundant crinoid fragments. These open marine faunas were dated Sinemurian to early Pliensbachian (Duffaud, 1960; Du Dresnay, 1988). This formation is absent in the south and east part of the basin where the first recorded Jurassic formation, namely the

Amsittène Formation, is composed of Toarcian continental deposits (Duffaud, 1960, Adams et al, 1980), interpreted as braided rivers, lakes and lagoons and flood plain deposits (Ambroggi, 1963; Bouaouda, 2004; Ouajhain et al., 2011).

The base of this formation is erosive and locally cuts down to the CAMP basalt and the Triassic. The Toarcian stage records an overall transgression across the basin and the appearance of a second carbonate formation, the Tamarout Formation. This formation is composed of shallow marine to sabkha deposits, including oolites, carbonate mudstones, stromatolites and dissolution–collapse breccias or evaporites (Ambroggi, 1963; Adams et al., 1980; Peybernès et al., 1987). The Middle Jurassic record shows a second major period of siliciclastic sedimentation form the Aalenian to the Bathonian. This interval is dominated by siliciclastic deposits in most of the study area and referred to as the Ameskhoud Formation (Adams et al., 1980; **Fig. 1b**). It can be noted that in the north of the study area, the same period records the development of evaporites and dolomites and evaporites, similar to the lithology of the Tamarout Formation, and is referred to by some authors as the Id ou Moulid Formation (Peybernès et al., 1987). In the centre and eastern part of the EAB, the Ameskhoud Formation is dominated by red clay and siltstones with sandstones and conglomerates intercalated (Ambroggi, 1963; Adams et al., 1980; Bouaouda, 2004). The Ameskhoud Formation presents a pronounced SE/NW orientation, where the proximal siliciclastic deposits are observed in the east and south of the basin and the marine influence is more noticeable as the outcrops are further towards the NW (Ambroggi, 1963; Duval-Arnould, 2019). The depocenter of the Ameskhoud Formation would therefore be located towards the SE of the central part of the basin (**Fig. 1a**, Imouzzer), where the sedimentation is essentially composed of marine siliciclastics. During the end of the Middle Jurassic, the transgression initiated during the Bathonian allows the development of initially oolitic grainstones, then Brachiopod-rich floatstones and finally marls all over the EAB (Ambroggi, 1963; Ager, 1974). This widespread succession is named the Ouanamane Formation (Adams, 1979; Adams et al., 1980) and has been dated Bathonian to Middle Oxfordian (Olivier et al., 2012). The following Lalla Oujja Formation (Adams, 1979) is dominated by coral-rich deposits, locally encrusted by microbialites and dolomitized, dated middle Oxfordian to Kimmeridgian (Ambroggi, 1963; Adams, 1979; Martin-Garin et al., 2007; Olivier et al., 2012). Directly following the coral build-ups succession, the Iggui El Behar Formation is composed of mud-supported carbonates with

sparse fauna including large benthic foraminifera, locally, it also comprises some stromatolites and traces of evaporites (Ambroggi, 1963; Adams, 1979). This formation has been largely interpreted lagoonal, intertidal to supratidal deposits (Adams et al., 1980; Bouaouda, 2004).

The Kimmeridgian period is dominated by fluvial deposits in the eastern part of the basin, and in the centre and west of the basin by red marls and clays, called "Marnes Chocolat", with intercalated thin marine carbonates beds (Ambroggi, 1963; Duffaud et al., 1966; Adams et al., 1980; Bouaouda, 2004). The last Jurassic stage is marked by renewed carbonate deposition, named the Tismerroura Formation (Adams et al., 1980). This Tithonian succession is subtidal to supratidal. It is composed of a thick evaporitic succession in the area of Imi'N Tanoute, in eastern-most part of the basin (Duffaud et al., 1966; Duval-Arnould, 2019), while in all other locations, it is composed of micrites, oolites, stromatolites, dissolution breccias, with some bioclastic intervals, intercalated with rare thin beds of red clay (Duval-Arnould, 2019).

2.2.3. Early Cretaceous

Sedimentation during the Lower Cretaceous in the EAB was dominated by inner to outer shelf-open marine conditions. Pioneering work by Roch (1930), Ambroggi (1963), and Duffaud et al (1966) produced a lithostratigraphic framework for the basin and the assignment of dedicated formation names (**Fig. 1**). These mixed carbonate-clastic deposits are rich in marine fossils and have been dated using mainly ammonoids (Rey et al., 1988; Wippich, 2001; Ettachfini, 2004; Company et al., 2008; Luber et al., 2017; Bryers et al., in progress) but additionally echinoderms (Rey et al., 1988; Masrour, 2004) and calpionella microfossils (Taj-Eddine, 1992).

Lower Cretaceous deposits mostly thicken towards the west (i.e., basinwards) and some formations disappear towards the east (proximal) as a result of coastal onlap (Rey et al., 1986). Sedimentary geometries are broad and low-relief on the shallow dipping marine shelf with limited syn-sedimentary folding observed. However, thickness variations are seen where outcrops thin and appear to pinch out towards pre-existing topographic highs inherited from the underlying structural configuration of the Jurassic (Rey et al, 1986; Luber et al., 2019).

The lowermost formation of the Cretaceous is the Agroud Ouadar Formation, dated as Lower to Upper Berriasian, and consists of silty limestones and marls rich in echinoids, oysters, bivalves and brachiopods. This is followed by the Sidi L'Housseine Formation that is constrained to Lower Valanginian to lowermost Hauterivian age and represented by marls interbedded

with bioclastic limestones. Towards the top of the formation, the beds become siltier and thin sandstones are observed. Overlying this is the Tamanar Formation, of strictly a Lower Hauterivian age, made up of massive coral-rich limestones followed by sandy bioclastic limestones and laminated calcareous sandstones. The following succession, the Talmest Formation, consists of marls interbedded with bioclastic and silty to sandy limestones rich in oysters, becoming increasingly more marl-dominated vertically and is aged as Upper Hauterivian. The Lower to Upper Barremian-aged Taboulaouart Formation above is quite similar in lithology, being made up of marls interbedded with bioclastic limestones. The Bouzergoun Formation lies above this and is dated as Upper Barremian to lowermost Aptian. It starts with thick shelf-derived mudstones and minor sandstones which are then cut by a clear ravinement surface containing shallow marine sandstones and coarse fluvio-deltaic sandstones and terminates with interbedded sandstones, sandy limestones and marls. Overlying the Bouzergoun are the Tamzergout (Aptian) and Oued Tidsi (lower Albian) Formations respectively, which are dominated by marls and occasional bioclastic limestones.

2.2.4. Late Cretaceous

A significant increase in subsidence in the Cenomanian (Zühlke et al., 2004) resulted in a basin-wide transgression represented by marls and limestones of an outer shelf environment (Ait Lamine Formation; **Fig. 1b**). The transgressive trend continued in the start of the Turonian in which organic-rich, basinal, black shales are recorded (Ferry et al., 2007). The latter part of the Turonian shows a return to shallower platform conditions indicated by dolomitic calcarenites (Ferry et al., 2007). This regression continued into the Coniacian (sandy dolomites, silts and evaporitic deposition) and the Santonian (shallow water limestones and marls in the west that move into deltaic silts and sands and evaporates in the east; Zühlke et al., 2004). The end of the Cretaceous is marked with a transgression between the Campanian to Maastrichtian. The Campanian consists of inner to outer shelf derived dolomites and marls and the overlying Maastrichtian is represented by shallow marine limestones and marls, which in a proximal direction shift to phosphate-enriched siliciclastic sandstones (Zühlke et al., 2004).

2.3. Mesozoic growth of the anticlines

In the literature, Jurassic to Cretaceous paleo-highs, evaporite mobilisation and/or structural folding in the EAB has been suggested and locally documented (Rey et al., 1988; Stets, 1992; Bertotti and Gouiza, 2012; Luber, 2017; Jaillard et al., 2019). In the Tidsi anticline, the presence of a diapir has been imaged on seismic (e.g., Hafid et al., 2000) and it is now well documented that halokinesis started as early as the Early Jurassic (Hafid et al., 2006; Hafid et al., 2008). However, the anticline lies in the basinal domain of the EAB (Frizon de Lamotte et al., 2008), as opposed to the other anticlines exposed in the WHA, mostly because of an N-NE/S-SW fault east of the Tidsi anticline (East Necnafa fault; structure directly east of the anticline in **Fig. 1a**; Frizon de Lamotte et al., 2008). Field evidence, such as sedimentary wedges in Lower Cretaceous rocks suggests salt accommodate horizontal compression active in the Jurassic (Bertotti and Gouiza, 2012)

A recent study in the Jbel Amsittène, one of the Western High Atlas anticlines, reveals the fold grew during the Late Jurassic and Early Cretaceous by N-NW/S-SE horizontal shortening (Fernández-Blanco et al., 2020). Their detailed structural analysis leads to the characterization of the anticline as a fold-propagation fold verging north. This, together with syn-tectonic wedges at outcrop and anticline scales suggest a minimal influence of evaporite withdrawal on the initial growth of the Amsittène, and its early development by contractional tectonics (see Fernández-Blanco et al. (2020) for additional arguments and complete discussion). They concluded that most of the folding that led to the anticline current geometry took place during the Alpine contraction.

The Imouzzer anticline, oriented SW/NE, is part of a larger E/W anticlinorium that extends from the Triassic Argana valley to the Atlantic coast and also contains the Cap Rhir and Anklout anticlines (**Fig. 1c**). The orientation of the Imouzzer has been attributed to basement structures, possibly rift-related (Ager, 1974). Cap Rhir has been more recently studied (Martin-Garin et al., 2007; Duval-Arnould, 2019) and analyses of Jurassic facies reveals the presence of a tilted block as a paleo-topographic constrain for the growth of a reef. Extensive facies analyses of Lower Cretaceous sediments around Cap Rhir suggests that it was forming a paleo-high during the Barremian-Aptian (Luber, 2017).

The Jurassic facies of the Imouzzer, Anklout and Lgouz anticlines were studied and added to a review of previous works in Duval-Arnould (2019). The orientation of later two anticlines is the

result of that of basement structures (Ager, 1974). Shortening in the Anklout anticline, extracted from on Jurassic bed length, is estimated at ~10% (Frizon de Lamotte et al., 2000). The Lgouz and the Amsittène anticlines display an overturned southern and northern limb, respectively (Ambroggi, 1963; Ager, 1974).

3. Material and methods

The geologic horizons and markers were mapped out using previous cartographic information around the Amsittène and Imouzzer anticlines, and their geospatial position defined using Google Earth integrated with satellite images from the Shuttle Radar Topographic Mission (STRM) and its Digital Elevation Model (DEM), of 90 m spatial resolution and c. 16 m vertical error (Hoffmann and Winde, 2010; Rusli et al., 2014). Dip angles and azimuths were reconstructed at km-scale using a 3D plane-solver Google Earth plugin, developed by J. Jamieson and G. Herman (service was interrupted; http:// www.impacttectonics.org/ GeoTools/3pphelp.html). Stratigraphic boundaries are defined on remote sensing images on the basis of colour changes and interpolating (or combining) the geological contacts extracted from geo-referenced 1:50,000 geological maps (e.g., Jaidi et al., 1970). Selected stratigraphic logs (Table 1), serve as the basis for the defining main siliciclastic fluxes in the basin for the Jurassic and Cretaceous (Duval-Arnould, 2019; Bryers, in progress; respectively). To check the quality of this data set and complement it, field measurements (contact coordinates and attitudes) were taken locally from both anticlines studied (Tables 2 and 3). This allowed correction of the DEM in Google Earth, which has been noted by previous authors to not always yield accurate results for steep slopes (Richard and Ogba, 2016).

Geometrical consistency of structural cross-sections was tested using two dimensional restorations (Dahlstrom, 1969; Elliot, 1983; Mitra and Namson, 1989; Durand-Riard et al., 2010), using the Move 2D software from Midland Valley. This study preserves the thickness of marine-dominated rocks and uses flexural slip unfolding (Moretti, 2008) to rotate fold limbs to a horizontal datum or an assumed regional surface. Flexural slip is removed during rotation of fold limbs by layer-parallel shear and according to a defined fold axis (based on the orientation of the beds in each of the fold flanks). During flexural slip unfolding, line length is preserved and true bed thickness is constant, leading fold area conservation in the section direction (Moretti, 2008), which is likely different but somewhat similar than the unfolding direction. However, it is important to note that the unfolded horizons and related sediments are not uncompacted.

For the sedimentary logs collected from and around the anticlines, the identification of the carbonate facies is based on the Embry and Klovan (1971), extension to the Dunham (1962) classification. The siliciclastic descriptions are based on textural classification, the grain size

grades follow the scale defined by Wentworth (1922) and the textural classes from Folk (1980). Finally, a correlation is constructed between the Jurassic sediments of the Imouzzer and Amsittène anticlines by using two exploration wells (**Fig. 1**; TMS-1 and TMR-1). These two wells are located at the crest of an anticline of lesser magnitude, which is part of the larger Haha syncline (e.g., Piqué et al., 1998).

4. Thickness changes around the anticlines

4.1. Amsittène

The ENE-WSW-striking Amsittène Anticline is a c. 40 km-long asymmetric fold (Fernández-Blanco et al., 2020; **Fig. 2**). The Oxfordian beds in the fold northern limb are overturned in the west of the fold, with S-SE dips up to 40°, and dip 20°-30° to the N-NW in the east of the structure (**Table 2**). In combination with the constant dip angles of 25 to 30° S-SE along the southern flank, we constrain the axial plane that dips c. 85° towards the S-SE. Halokinetic effects are only observed in the west of the anticline, where a diapiric Triassic evaporite outcrops leads Jurassic layers to dip away from it. Thickness variations in the Middle Jurassic (also called Dogger in the area, although it only refers to Aalenian to Bathonian stratigraphy) to the Tithonian formations along lines following the scalped anticline show an overall thickness decrease from the northern flank towards the east (**Fig. 2c**; already published in Fernández-Blanco et al., 2020). From the 2D restoration, we recover a tectonic shortening of 7.5-13% along the cross-section direction (perpendicular to fold axis) that is consistent with previous estimates (Fernández-Blanco et al., 2020).

In the southern limb, all formations progressively increase in thickness to the west (**Fig. 2**), which is explained by the fact that the EAB develops as an overall carbonate ramp (e.g., Jaillard et al., 2019). The Callovian, the Oxfordian and the Kimmeridgian thicken westward along the southern limb to (with thicknesses changing from c. 50 to 140-200 m, c. 140 to over 300 m, and c. 80 to 100 m respectively). Profiles A and B show northward thickening for all horizons, when restored to the Oxfordian (**Fig. 2a**).

On the northeastern side of the anticline at the marked location (fig.3; **Fig. 2**), a cliff of c.15m of Aalenian to Callovian limestones, shows discontinuous layers forming onlaps (**Fig. 3**). Onlaps occur towards the south, i.e., the center of the anticline. These onlaps result in a thickening of more than 5 m over a distance of about 50m towards the north (**Fig. 3b**). This results in a change in dip from 25° in the upper section to 15° in the lower section.

Stratigraphy	Dip angle [º]	Dip azimuth [º]	Limb	Latitude [decº]	Longitude [decº]	Elevation [m]	Acquisition
Dogger	13	141	S	31.170	-9.647	843	digital
	30	339	N	31.194	-9.613	659	digital
	21	330	N	31.184	-9.651	656	digital
	14	345	N	31.184	-9.664	571	digital
	19	22	N	31.193	-9.597	816	field*
Callovian	25	162	S	31.156	-9.667	640	digital
	17	153	S	31.162	-9.652	768	digital
	22	154	S	31.163	-9.645	735	digital
	19	160	S	31.173	-9.623	801	digital
	47	158	N	31.192	-9.636	644	digital
	64	172	N	31.189	-9.650	477	digital
	48	175	N	31.187	-9.657	424	digital
	49	338	N	31.197	-9.621	511	digital
	15	14	N	31.199	-9.595	633	field
Oxfordian	31	166	S	31.154	-9.667	601	digital
	35	164	S	31.152	-9.667	540	digital
	33	159	S	31.155	-9.661	627	digital
	33	164	S	31.158	-9.651	682	digital
	31	161	S	31.159	-9.644	621	digital
	25	155	S	31.161	-9.644	681	digital
	28	162	S	31.162	-9.636	695	digital
	25	164	S	31.165	-9.629	731	digital
	24	163	S	31.168	-9.629	798	digital
	21	162	S	31.167	-9.617	712	digital
	22	165	S	31.168	-9.611	686	digital
	16	149	S	31.175	-9.599	762	digital
	17	166	S	31.178	-9.591	768	digital
	11	138	S	31.185	-9.582	804	digital
	50	161	S	31.193	-9.633	546	digital
	86	155	N	31.192	-9.628	636	digital
	70	175	N	31.185	-9.666	514	digital
	16	13	N	31.197	-9.584	740	digital
	22	349	N	31.200	-9.605	633	digital
	22	189	N	31.191	-9.640	480	digital
	35	16	N	31.195	-9.595	779	field
Kimmeridgian	13	163	S	31.175	-9.580	581	digital
	33	163	S	31.156	-9.644	480	digital
	44	340	N	31.198	-9.611	607	digital
	46	171	N	31.189	-9.649	459	digital
Tithonian	23	168	S	31.151	-9.643	366	digital
	40	162	S	31.150	-9.667	444	field
	46	343	N	31.202	-9.612	523	digital
Jur./Cret.	34	161	S	31.147	-9.666	420	field

Table 2 | Digital (Google Earth) and field dip measurements of beddings from the Amsittène anticline. Dogger: Aalenian-Bathonian. The elevation has been obtained using the GPS coordinates and combined with NASA SRTM3 DEM. Overturned strata are highlighted in grey. *average of four field dip measurements from the location shown in **figure 3a**.

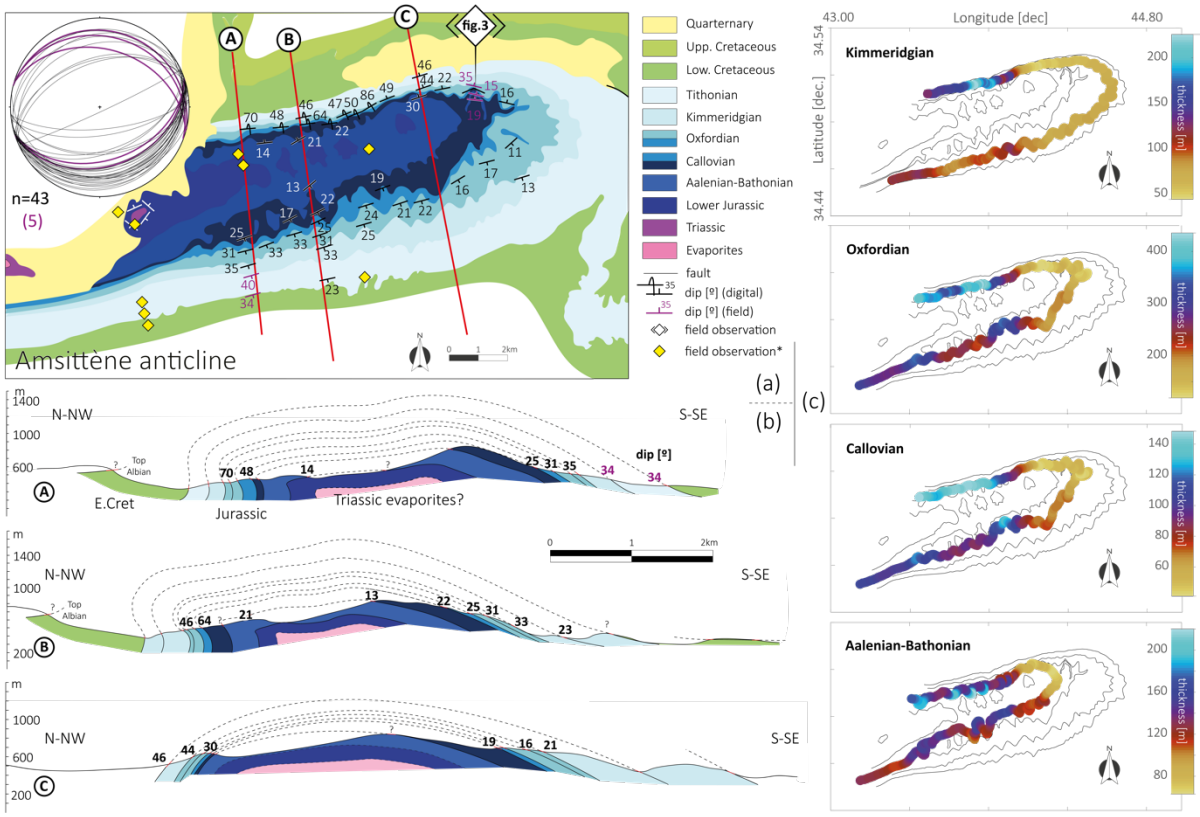

Figure 2 | a) Geological map of the Amsittène Anticline based on Google Earth mapping and Tamanar geological map (Duffaud, 1964). See the **table 2** for dip measurements of the Mesozoic sedimentary rocks. The stereoplot displays the field measurements in purple and the digital ones in black. Photographs from the marked location are displayed in **figure 3**. * Field observations in Blanco-Fernandez et al. (2020). b) Cross-sections A, B, and C, running perpendicular to the fold axis, without vertical exaggeration. c) Resulting thickness maps for Middle and Upper Jurassic units using the Paradigm Gocad® 'kine3d-1' tool (maps are published in Fernandez-Blanco et al., 2020; see details therein). The resolution of the thickness maps suggests a precision of around 20 m and lies below the thinnest formations modelled in the anticline. Note that each map displays the thickness along a line where the formation is outcropping with a similar line thickness for visualisation purposes only.

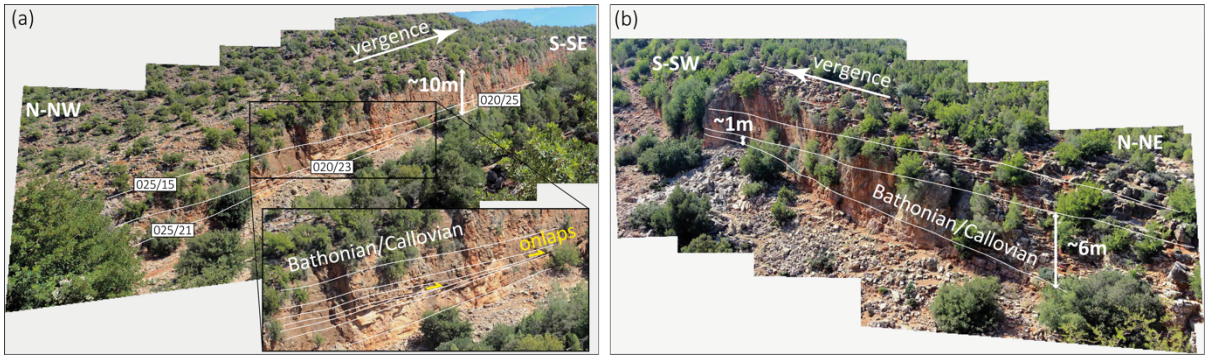

Figure 3 | Two sides of the same valley in the northeast of the Amsittène anticline exposing Bathonian/Callovian carbonates. The western side (a) highlights onlap structures, while its eastern counterpart (b) shows clear thickness variation in the Callovian, with thinning towards the anticline core. Note that the dip measurements were not added in **table 2** and **figure 4**, but only their average, given their close proximity, was used (022/19).

4.2. Imouzzer

The NE/SW striking Imouzzer periclinal anticline is c. 15 km long with two closures (in the SW and NE; **Fig. 4**), with Jurassic and Cretaceous rocks folded asymmetrically (**Table 3**). Thick layers of evaporite (gypsum) are deforming or locally interbedded in carbonate layers of the Toarcian (**Fig. 5**; Ambroggi, 1963). Syn-sedimentary onlap structures, normal faulting and asymmetric sedimentary thinning, as observed in the field, suggest active evaporite diapirism during the Early and Middle Jurassic. Thicknesses in the Aalenian-Bathonian sediments vary slightly along the anticline axis and range from c. 150 to 330 m (**Fig. 4c**). The thickness of Callovian rocks average 80 m and remains relatively constant throughout the profiles, except for thickening near evaporite outcrops. Thus, this horizon does not follow the thickness trends observed for Aalenian to Bathonian rocks (**Fig. 4c**). No thickness variations were calculated for Oxfordian and Kimmeridgian stratigraphic units, since their data points are too few and far apart to provide meaningful results.

Results of the structural geometry show a clear difference in the deformation on the Lower Jurassic unit, especially when compared to that of the Aalenian-Bathonian (**Fig. 6**). Unfolding of NW/SE cross-sections show that shortening varies between ~9.5 and 6%. Evaporite layers are dipping NE following the morphology of the fold core. Deformation of the Toarcian carbonate layers interbedded in the evaporite are found all along the breached valley, showing

multiple folding structures (Figs. 5a and b). The thickness of some evaporite bodies can be assumed to amount at least to 50 m where the base of the evaporite could not be located.

The Callovian carbonates, fairly constant in thickness, show little horizontal facies variation where exposed in Imouzzer, and a homogeneous evolution vertically. This suggests that Callovian-Oxfordian rocks were deposited horizontally atop a peneplained Lower Jurassic anticline, however no field evidences of emersion or erosion were observed. In the Northern part (Fig. 5c), Aalenian-Bathonian sedimentary rocks dip 68° N-NW, forming a conformable contact with the Callovian. The limestone layers within the Middle Jurassic are at an angle of approximately 30° with the Callovian to the north, meaning that the Aalenian-Bathonian siliciclastics between the Middle Jurassic carbonates might have 'corrected' this structural dip when the Callovian was deposited, potentially due to a pause in the evaporite mobilisation

The marly to sandy deposits of the Middle Jurassic, with thicknesses of 200 to 250 m, are strongly deformed. Folding is observed at the base whereas towards the top deformation features are of a faulted nature, showing normal faulting and smaller fold structures (Fig. 5d). Subtle changes (cms) in thicknesses, from the layers shown in figure 5d, from S to N across a normal fault might indicate syn-sedimentary deformation.

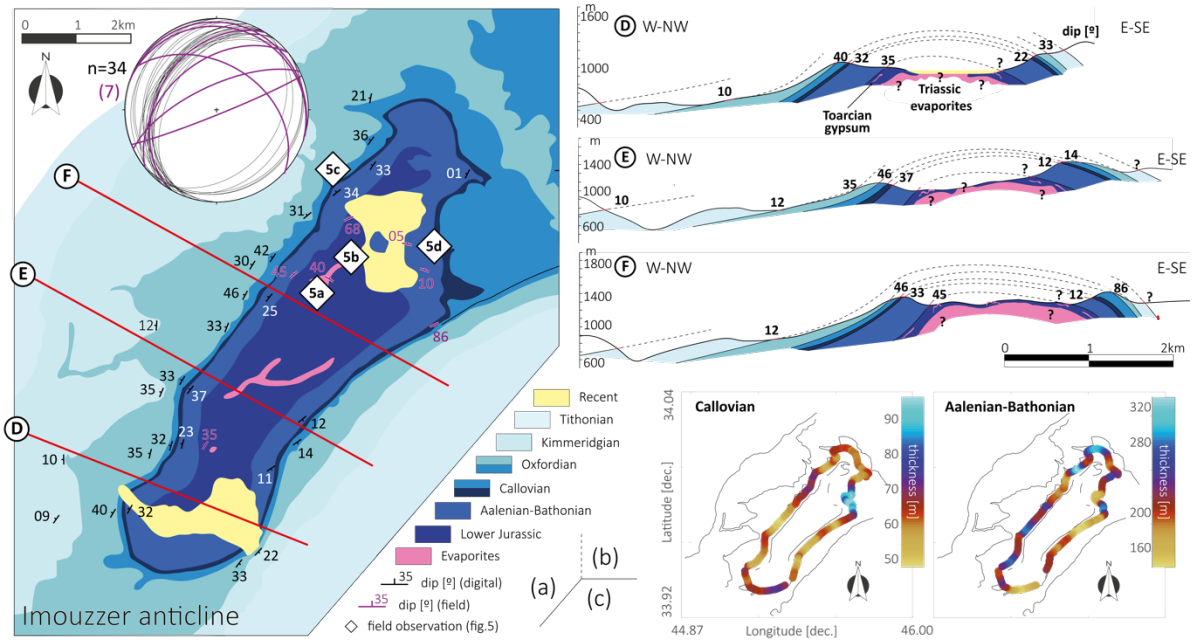

Figure 4 | a) Geological map of the Imouzzer Anticline based on Google Earth mapping and field observations. See the **table 3** for dip measurements of the Mesozoic sedimentary rocks. The stereoplot displays the field measurements in purple and the digital ones in black. Photographs from the marked locations are displayed in **figure 5**. b) Cross-sections D, E, and F, running perpendicular to the fold axis. C) Resulting thickness maps for Middle Jurassic and Callovian units using the Paradigm Gocad® 'kine3d-1' tool.

Stratigraphy	Dip angle [º]	Dip azimuth [º]	Limb	Latitude [decº]	Longitude [decº]	Elevation [m]	Acquisition
Lias	35	302	NW	30.691	-9.488	1070	field
	40	50	NW	30.714	-9.472	1258	field (Fig. 5a)
Dogger	23	285	NW	30.692	-9.493	1231	digital
	37	308	NW	30.698	-9.492	1002	digital
	32	299	NW	30.682	-9.502	927	digital
	45	321	NW	30.716	-9.475	1298	field
	68	335	NW	30.723	-9.463	1069	field (Fig. 5c)
	25	299	NW	30.714	-9.477	1361	digital
	34	321	NW	30.727	-9.468	1098	digital
	33	309	NW	30.731	-9.459	1121	digital
	10	19	SE	30.715	-9.450	1427	field
	5	20	SE	30.716	-9.451	1417	field (Fig. 5d)
	1	296	SE	30.728	-9.444	1462	digital
	12	141	SE	30.694	-9.471	1341	digital
	11	146	SE	30.688	-9.476	1276	digital
Callovian	34	321	NW	30.727	-9.468	1098	digital (Fig. 5c)
	86	158	SE	30.709	-9.449	1407	field
Callovian-Oxfordian	36	307	NW	30.733	-9.462	1216	digital
	42	306	NW	30.718	-9.478	1227	digital
	33	301	NW	30.700	-9.494	941	digital
	32	290	NW	30.692	-9.496	1179	digital
	14	145	SE	30.692	-9.472	1336	digital
Oxfordian	21	280	NW	30.742	-9.461	1124	digital
	40	301	NW	30.681	-9.504	1018	digital
	31	310	NW	30.725	-9.472	1196	digital (Fig. 5c)
	35	289	NW	30.699	-9.498	967	digital
	30	300	NW	30.718	-9.481	1141	digital
	46	299	NW	30.713	-9.484	1140	digital
	33	290	NW	30.708	-9.487	1166	digital
	33	127	SE	30.675	-9.482	1112	digital
	22	122	SE	30.677	-9.479	1131	digital
Kimmeridgian	9	305	NW	30.678	-9.509	897	digital
	10	270	NW	30.685	-9.508	700	digital
	35	295	NW	30.690	-9.500	959	digital
	12	272	NW	30.708	-9.499	821	digital

Table 3 | Digital (Google Earth) and field dip measurements of beddings from the Imouzzer anticline. The elevation has been obtained using the GPS coordinates and combined with NASA SRTM3 DEM.

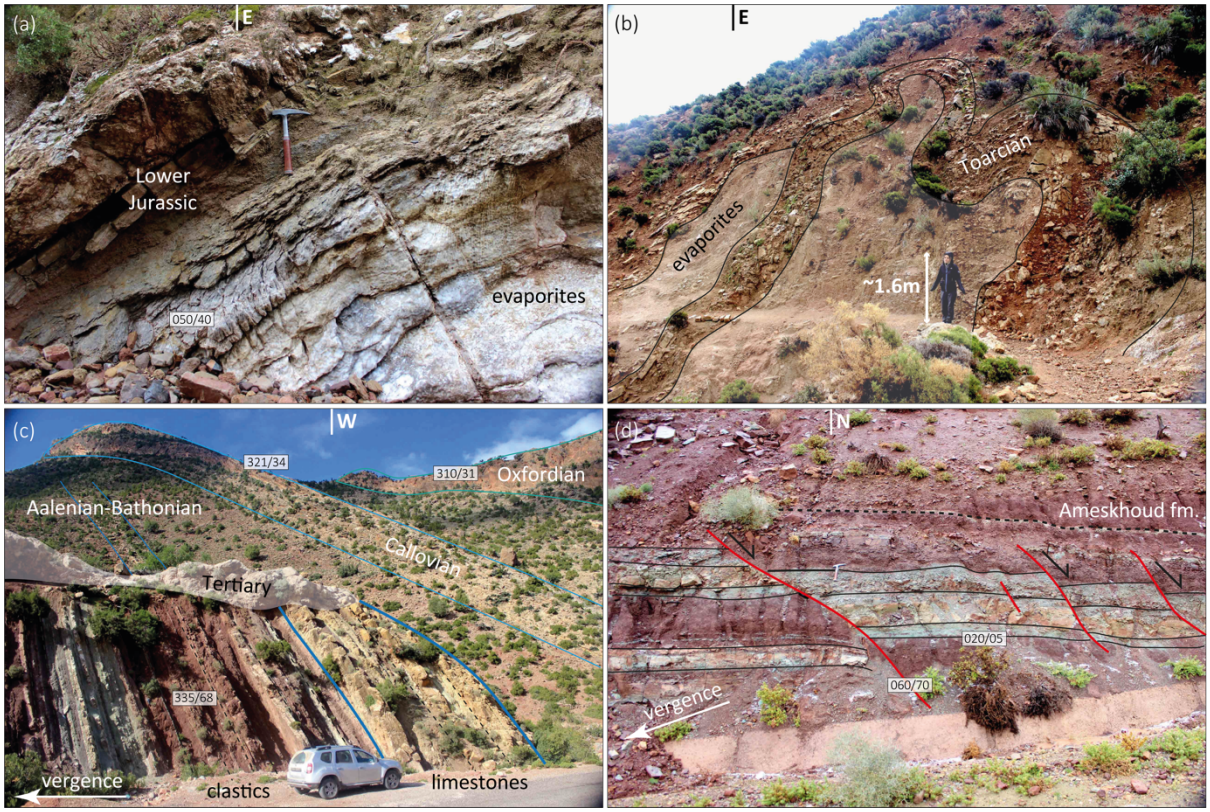

Figure 5 | Field observations from the Imouzzer anticline with locations marked in figure 4. a) Triassic or Lower Jurassic evaporites near the core/NW limb of Imouzzer anticline. b) Toarcian sediments heavily folded (i.e., unconsolidated?) related to the mobilisation of Toarcian(?) evaporites. c) Along-strike thickness variations in the upper Middle Jurassic ('Dogger')/Lower Callovian(?) sediments. d) Localized normal faulting in fine clastic Middle Jurassic layers.

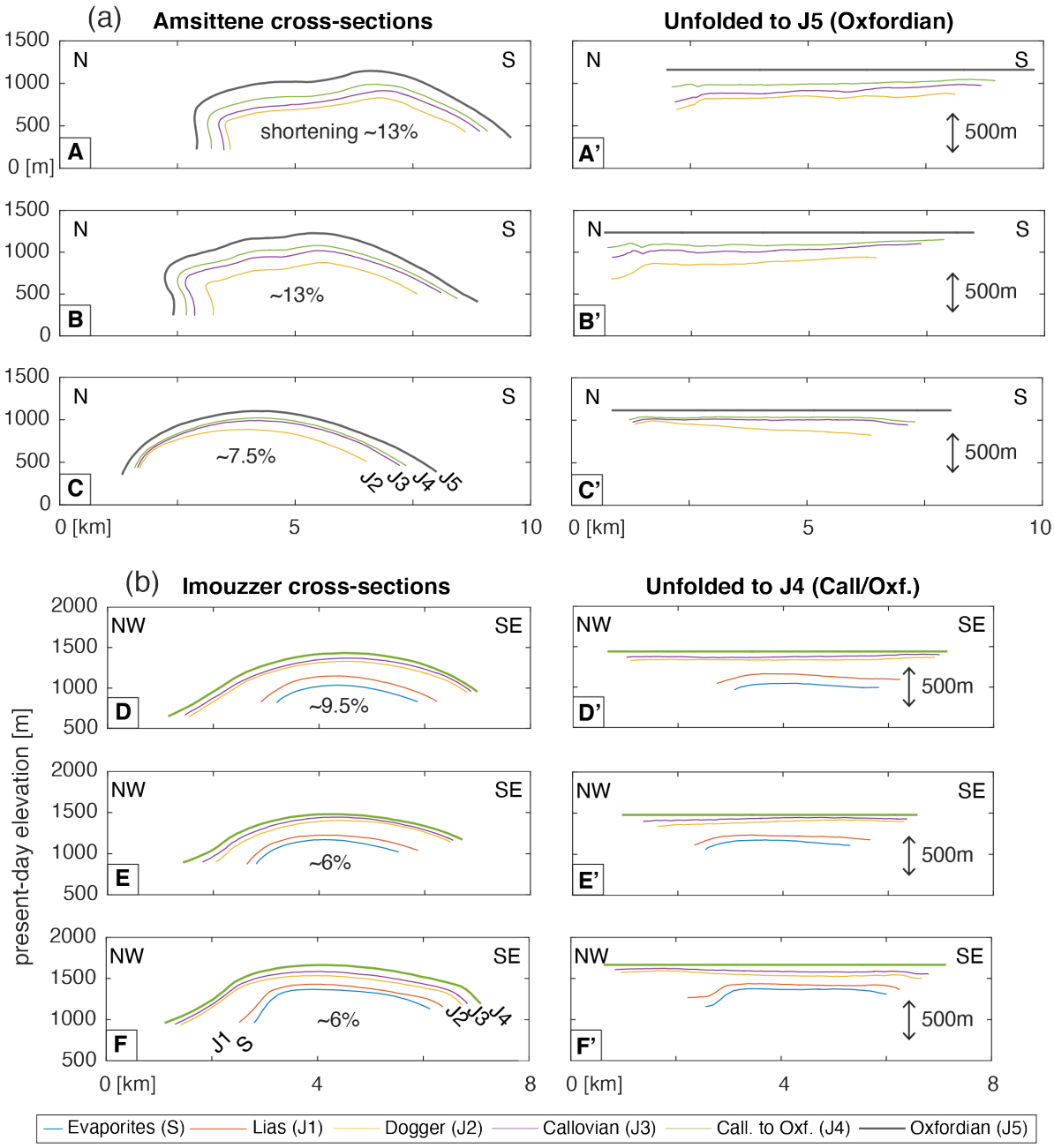

Figure 6 | Cross-sections and restoration to the Oxfordian (J5-4; top of the stratigraphic units) using 2D Move® for a) Amsittène and b) Imouzzer anticlines. No vertical exaggeration. Note that Aalenian-Bathonian (Dogger) and Callovian have been historically differentiated in the area (Ambroggi, 1963; Adams et al., 1980).

4.3. Correlation between the anticlines

Unfolded sections in the WHA anticlines points towards syn-sedimentary thickness variations of Jurassic sediments at these locations. To shed light on the evaporite activity in the platform domain of the EAB, it is important to understand the regional thickness changes, especially away from, and in between, the anticlinal structures (Fig. 1c). A strong increase in thickness in between anticlines could indicate the formation of mini-basins due to active evaporite mobilisation during forming anticlines. It is noteworthy that the wells were drilled atop a smaller anticline than Amsittène and Imouzzer. However, assuming that the size of the presently exposed anticlines is an indication of their importance in the Jurassic, there could be some substantial thickness variations.

Therefore, two wells located in the northern portion of the 50 km wide Haha syncline have been used to create a ~N/S correlation for the Triassic to Kimmeridgian (Fig. 7). The stratigraphic logs of the two wells, namely Tamanar 1 (TMR-1) and Timsiline 1 (TMS-1), were provided to the present authors by the OHNYM. The correlation panel shows no large thickness gradients, indicating that there was no substantial diapir forming the two anticlines, i.e., ones that would be comparable to the EAB offshore or the Tidsi anticline (Fig. 1), nor mini-basins forming in between the above studied anticlines. Instead, the Aalenian-Bathonian, Callovian and Oxfordian stratigraphic units are surprisingly constant in thickness. Only the Lower Jurassic (also referred to as Lias) is substantially thickening away from the Amsittène anticline towards the south (from ca. 350 to 800 m), although information on the Lower Jurassic thickness is missing from the Imouzzer anticline. Still, Early to Middle Jurassic stratigraphic units thin towards the anticlines (where they locally have a fairly consistent thickness; see previous parts), which is in line with a pre-Alpine growth of the folds.

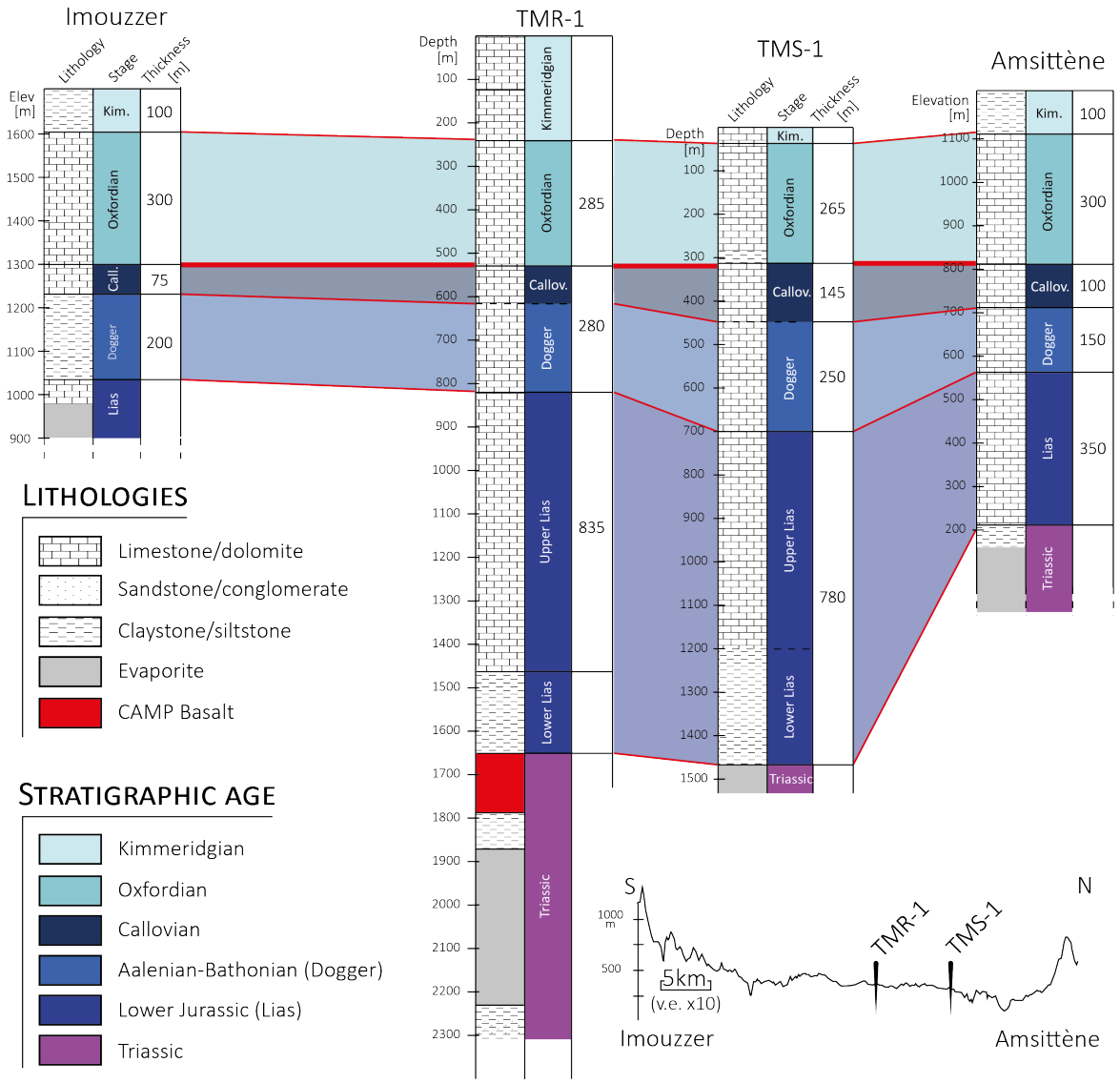

Figure 7 | South-north well correlations between Amsittène and Imouzzer anticlines. The anticline core series flattened to the top-Callovian as it is a clear geological marker in all studied areas and with present-day elevation profile (inset). The two wells used were drilled on a smaller anticline where the Jurassic is partially exposed (**Fig. 1c**).

5. Siliciclastic influx around the anticlines

5.1. During the Middle and Upper Jurassic

Along the Imouzzer and Amsittène anticlines, variations in the amount of siliciclastic flux have been recorded (Duval-Arnould, 2019; **Fig. 8**). The Aalenian to Bajocian/Bathonian period is marked by the deposition of thick continental and marine siliciclastics in the East and South of the EAB (Jurassic "Sa" in ASH; Sa – for Siliciclastic Ameskhoud Fm; see **Table 1** for coordinates). The north-western part of the basin (Amsittène Anticline) in the same period is dominated by carbonates and evaporites. These lateral facies variations indicate an E/W or SE/NW siliciclastic system orientation during this period. During the Callovian, the siliciclastics flux in the basin decrease, and the sedimentation is dominated by carbonates until the Middle/Upper Oxfordian.

During the Callovian, an important sedimentological aspect is reflected by the facies variation along the Amsittène anticline (Duval-Arnould, 2019). The southern flank Callovian deposits (**Fig. 8**, AMCA) record deeper facies and relatively deeper-water fauna (abundant ammonites) compared to the northern flank (AME). This indicates the presence of a topographic high associated with the northern part of the anticline. Potential evaporite movements might have occurred prior to the Callovian stage to create this high. The high could also have acted as a topographic barrier to siliciclastic deposits coming from the north during the same period (Jurassic "S1" in AME). The Callovian siliciclastics, associated to the siliciclastic pulse "S1"would have deposited in this shallower domain, and the topographic barrier could have prevented them to reach the other side of the anticline. This would have induced a re-routing of the Callovian siliciclastic sediments coming from the north east of the basin (Jurassic 'S1' in well NDK-2) towards the offshore to the west, guided by the northern flank of the Amsittène anticline. Dating of dinoflagellates cysts place the siliciclastic pulse "S1" during the Upper Callovian (Jaydawi et al., 2016). We can note that the well MKL10, initially dated Callovian to Upper Oxfordian has been reattributed to the Lower Callovian (Jaydawi et al., 2016) and the absence of siliciclastics in this particular well is therefore expected (Jurassic "S1" in MKL10).

The north and south of the Imouzzer anticline present fairly similar deposits thicknesses during the Callovian (Duval-Arnould, 2019). The absence of the siliciclastic influx "S1" along this anticline can be noted in locations, ASH, IMZ and TID (**Fig. 8**). The Callovian facies are

homogeneous along the anticline and followed by coral build-ups during the Oxfordian. This coral-rich unit is then interrupted in the north of the anticline by cross-bedded siliciclastic deposits.

Along the Imouzzer Anticline, the NW flank records siliciclastic deposits during the Middle to Upper Oxfordian (**Fig. 8**, Jurassic "S2" in ASH), which are absent along all the eastern flank of the anticline and in the SW part of the anticline (TID and IMZ). In the Amsittène anticline, a comparable Oxfordian siliciclastic influx is observable along the northern and southern flanks (Jurassic "S2" in AME and AMCA). This siliciclastic influx can be traced further to the North and East, in the wells NDK-2 and NDK-3 (Fig. 8b, Jurassic "S2" in NDK2 and NDK3). This siliciclastic influx "S2" takes place at the same stratigraphic position in the Amsittène and Imouzzer anticlines and have been therefore interpreted to be due to the same event linked to the exhumation of the Meseta (Charton et al., 2020).

The siliciclastic deposits on the north of the Imouzzer anticline and in the Amsittène anticline indicate high energy settings, potentially linked to their location on topographic highs. In the locations AMCA and ASH, the higher energy settings persist after the siliciclastic influx, and carbonate grainstones progressively replace the sandstones, before the onset of the generalized regression and the development of tidal-flat deposits all over the basin. In other locations, the transition is more abrupt and there is no record of high-energy transition facies between the deeper coral-rich unit and the tidal-flat deposits.

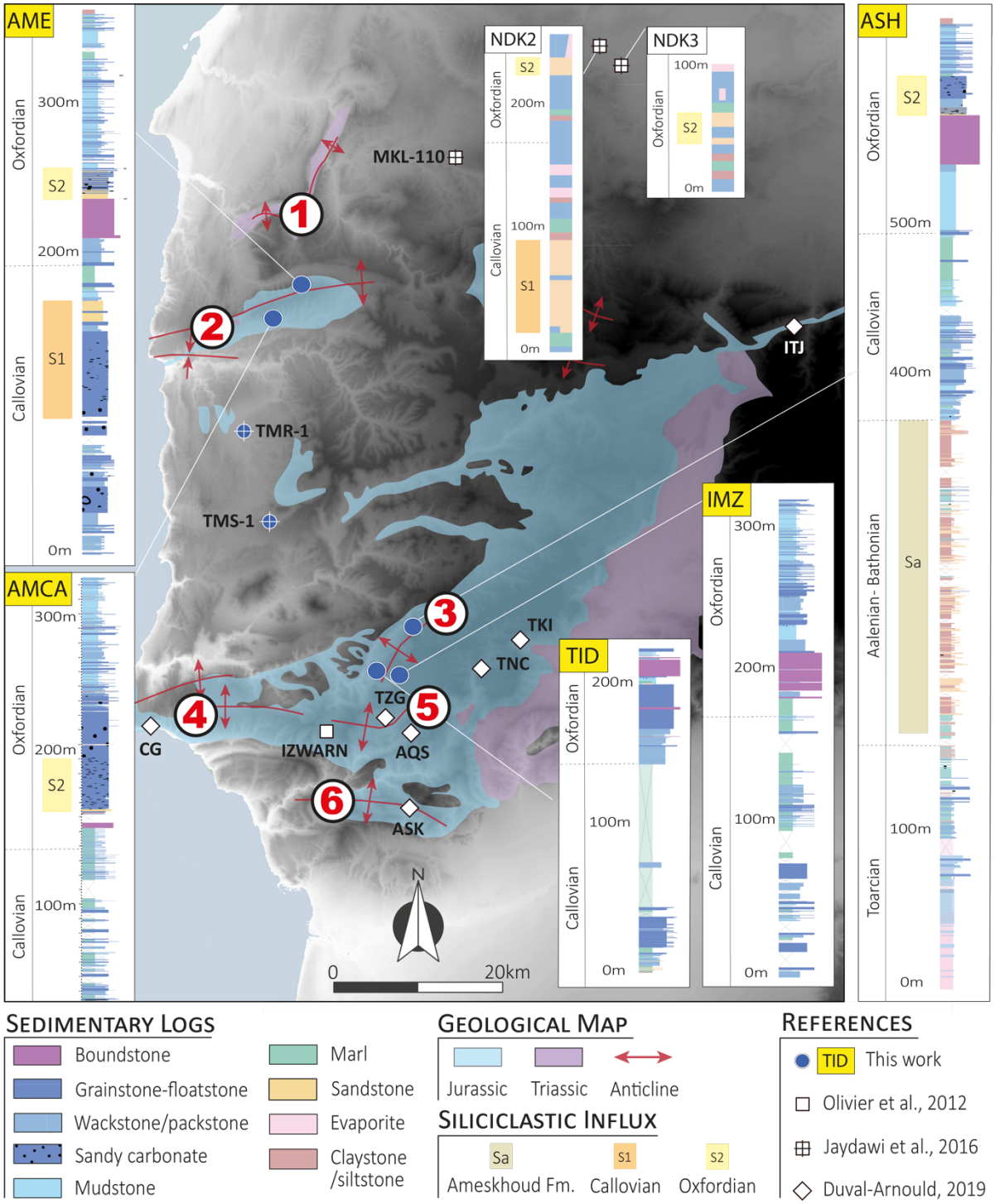

Figure 8 | Simplified logs from Jurassic outcrops in the studied anticlines and location of recent works (compilation after Duval-Arnould, 2019). Anticlines: 1. Tidsi, 2. Amsittène, 3. Imouzzer, 4. Cap Rhir, 5. Anklout, and 6. Lgouz. The mention of '0m' at the base of the logs is the base of the Callovian or Toarcian stratigraphic units (ASH).

5.2. During the Lower Cretaceous

The location and timing of Lower Cretaceous siliciclastic influx and their pathways are presented in the work of Luber (2017; **Fig. 9**). The first period of clastic influx is documented several kilometers inland of the Cap Rhir anticline (**Fig. 1c**; Cretaceous "S3"; see AH), and dated as Early Valanginian by recent biostratigraphy (Bryers, pers comm.), part of the Sidi L'Housseine Fm. The sandstones are interpreted as marine shoreface deposits with outcrop data indicating a N-NW/S-SE palaeoflow direction. The interval varies in thickness from 6 to 40 m (Ain Hammouch to Tamzargout localities). This sandstone interval is not documented north of Cap Rhir or on either side of the Amsittène anticline. Approximately 10 km northeast of Cap Rhir, a very thin interval (several 10s of cm thick beds) of calcareous sandstones is recorded interbedded with marls. They are very fine to fine grained, have flute mark scours on their bases and show no internal bedding structures. These sandstones are interpreted as minor confined shelfal turbidite flows, and the interval dated as Upper Valanginian (based on superposition amongst ammonite dated beds) is not recorded elsewhere in the EAB.

A second influx of clastics is recorded during the Lower Hauterivian (Cretaceous "S4"; constrained by ammonite biostratigraphy; Bryers, pers comm.). This incursion is found more frequently across the EAB than the Lower Valanginian episode, documented 2 to 3 km southeast of the Cap Rhir anticline (AH, Tamzargout Fm) and slightly north of it (see log IG; **Fig. 9**) and is also found adjacent to the Amsittène anticline (AMS-1) although strata preservation is quite poor due to alpine deformation. The facies is interpreted as a marine shoreface environment with a N-NW/S-SE palaeoflow and interval thickness varies from less than 2 meters (AMS-1 log) to ca. 10 meters (Ain Hammouch Fm).

A third, and particularly notable period of clastic input occurred during the Upper Barremian to Lower Aptian (Sb – for Siliciclastic Bouzergoun Fm; dated by recent biostratigraphy Luber et al., 2019). These are interpreted as fluvio-deltaic to shallow marine deposits that incise into the underlying Lower Cretaceous stratigraphy, forming a regional erosive unconformity as a result of a forced regression of the shoreline (Luber et al., 2019). Thickness variations of the Bouzergoun Fm (ca. 10 to 80 m) and variabilities in measured palaeocurrent directions suggest the influence of palaeohighs. For example, palaeocurrent data north and south of Cap Rhir indicate the local palaeohigh may have diverged sediments moving towards the basin into multiple transport pathways as well as providing additional local sediment input (Luber, 2017).

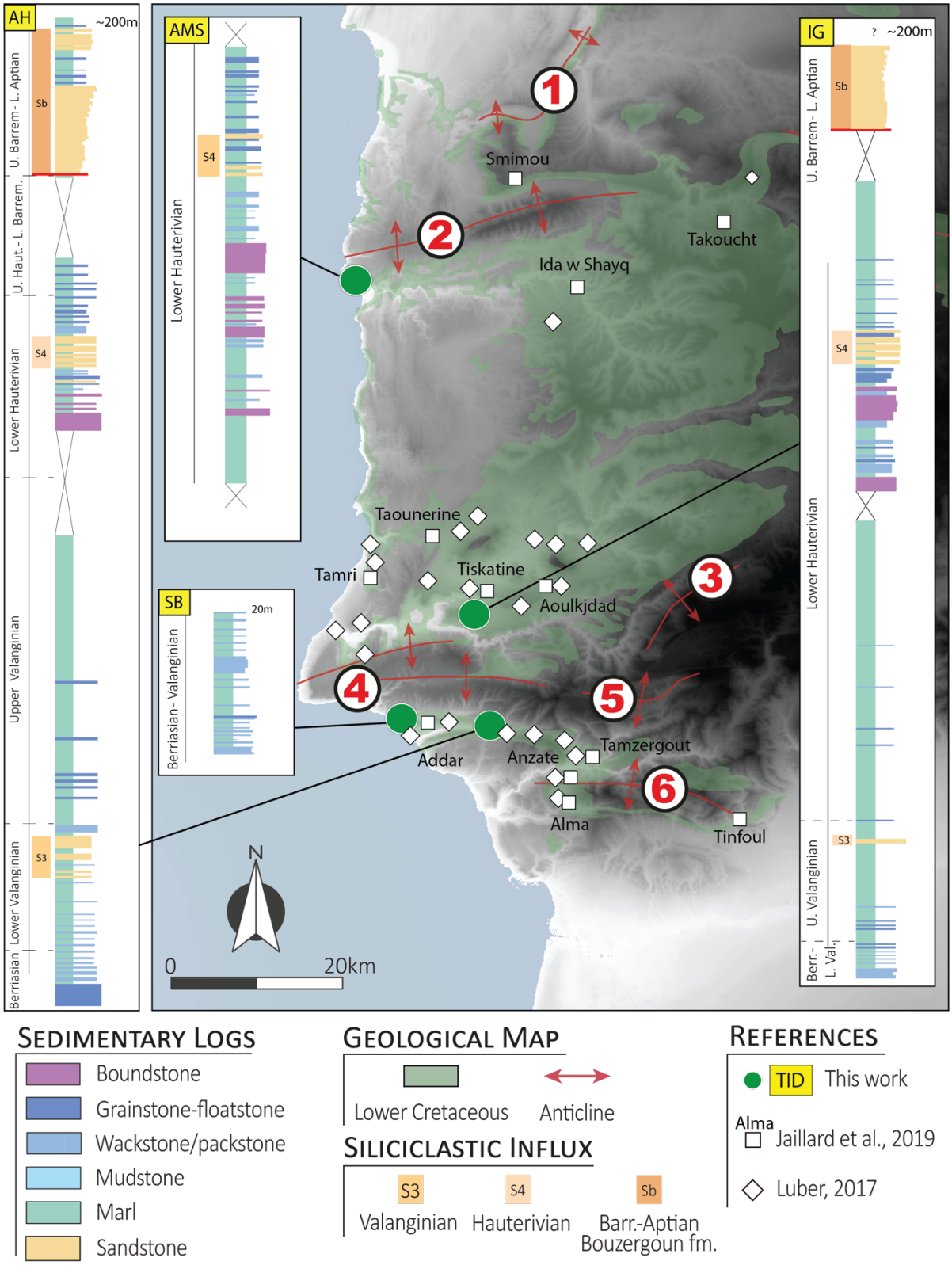

Figure 9 | Simplified logs from Cretaceous outcrops around the studied anticlines (compilation after Bryers, pers comm.). Anticlines: 1. Tidsi, 2. Amsittène, 3. Imouzzer, 4. Cap Rhir, 5. Anklout, and 6. Lgouz.

6. Implications and discussion

6.1. Evaporite mobilisation and mechanism

Early Mesozoic evaporite mobility is interpreted to have been instrumental in the formation of both anticlines from the Early and into the Middle Jurassic (**Fig. 10**). These evaporites were overlain by Late Jurassic carbonates which show systematic N-S and E-W thickness variations (**Figs. 2** and **4**). In the Amsittène anticline, Triassic evaporite mobilisation occurs from the Early to Middle Jurassic (**Fig. 10a**), and in the Imouzzer anticline (**Fig. 10b**) the Triassic and Toarcian(?) evaporites formed a bulge during the Early and Middle Jurassic (**Fig. 11a**), which strongly deformed the two sedimentary units and possibly led to crestal erosion with carbonate shedding.

In the Agadir-Essaouira Basin (EAB), folds expressed on the sea-floor led to the formation of large carbonate reefs and reef foresets (**Fig. 11a**; Duval-Arnould, 2019). Relatively-thin evaporites of Toarcian age interbedded in carbonate layers are in good agreement with the observations of thin evaporites causing structures dominated by narrow box-fold anticlines (Hudec and Jackson, 2007). The chaotic/tight folding patterns of evaporite deformation in the core of the Imouzzer anticline (**Figs. 5a-b**) could suggests that deeper, potentially Triassic, evaporite were mobile in the Lower to Middle Jurassic, especially during the deposition of the thick Aalenian-Bathonian Ameskhoud Fm.

This paper constrains the evolution of the Amsittène in the Early to Middle Jurassic and support that its growth is associated with halokinesis. Fernández-Blanco et al. (2020) constrains the evolution of the Amsittène in the Late Jurassic to Early Cretaceous, and support that its growth is associated with shortening tectonics. Irrespective of the triggering mechanism(s) for the growth of the folds, their effect is to partly compensate for the regional subsidence experienced by the EAB. This is justified by the fact that none of the stratigraphic intervals reviewed here document emersion, meaning the anticline tops never came above sea level in the Mesozoic. In other words, these regions only experience less subsidence than their surroundings.

Early and Middle Jurassic evaporite mobilisation in the Central High Atlas has been inferred from sedimentary onlaps described by Saura et al. (2014), Martin-Martin et al. (2017), and later reviewed in Moragas et al. (2018). While the evaporite mobilisation mechanisms in the

offshore EAB may differ from those onshore, timing of early evaporite mobilisation is similar (Neumaier et al., 2016; Pichel et al., 2019; **Fig. 11b**). N-NW/S-SE to N-NE/S-SW regional shortening is suggested for the Tidsi and Amsittène anticlines (Bertotti and Gouiza, 2012; Fernández-Blanco et al., 2020; respectively) to explain subsequent Middle Jurassic to Early Cretaceous syn-sedimentary deformations and anticline growth in the EAB and the exhumation in the basin hinterlands.

In the Lusitanian Basin (Portugal), salt diapirism has been identified during the upper Jurassic, which induced the formation of mini-basins. The structure of these mini-basins have been constrained through seismic stratigraphy and show important lateral thickness variations and onlaps against the salt structure during the Upper Jurassic, and minor evidences during the Early Cretaceous (Alves et al., 2002; Alves et al., 2003). Similarly, to the EAB, onlap geometries and quick lateral bedding dip changes have also been pointed out along some diapirs as markers of halokinetic movements (Davidson and Barreto, 2020). The Lusitanian Basin underwent similar evolution to the offshore EAB segment, which recorded halokinetics movements during the Middle Jurassic to Lower Cretaceous (Pichel et al., 2019).

During the Jurassic, coeval vertical motions resulted in subsidence of the EAB (e.g., Bertotti and Gouiza, 2012) and erosional exhumation of surrounding massifs, especially in the Anti-Atlas domain (**Fig. 11b**; e.g., Ghorbal, 2009; Gouiza et al., 2017; Charton et al., 2018), thereby leading to a topographic gradient (assuming exhumation is linked to uplift), and possibly a hydraulic head (salt/evaporite considered here as a fluid) gradient within the Triassic evaporites. Initially, mobile evaporite would then migrate N-NW, and traveling upward above structural features such as E/W Atlas rift related faults. Consequent evaporite lateral flow in the basinal domain of the EAB is interpreted to be one of the mechanisms that initiated the concomitant Jurassic folding and the migration of evaporite diapirs distally from east to west (Hafid et al., 2006; Tari and Jabour, 2013). Superimposed to the passive margin thermal subsidence, this is reinforcing the thickening of Jurassic successions towards the south-west, from near zero in the Argana Valley to ~1 km in the continental shelf break, (Zühlke et al., 2004). The Cretaceous series similarly thickens westward, from ~750 m east of the EAB to ~2.5 km (Zühlke et al., 2004). Westward thickening of Mesozoic successions corroborates the westward (High Atlas uplift; Stets, 1992) slope that may thus have led to lateral evaporite mobility and fold growth. Conversely, a potential northward slope caused by a Jurassic uplift

in the Anti-Atlas (e.g., Charton et al., 2018), south of the basin, would better explain the E/W fold growths that are observed here.

Alternatively, and although we favour the above-presented mechanism, evaporite mobilisation may be due to substantial temperature gradients in the evaporite bodies (i.e., thermal loading; Hudec and Jackson, 2007). Processes that could lead to such gradient include: i) extensive magmatic activity in the Late Triassic (Central Atlantic Magmatic Province; e.g., Davies et al., 2017) following the end of rifting, ii) by reactivation of ~NE/SW basement normal faults (e.g., Hafid, 2000; Piqué and Carpenter, 2001), as described for the offshore areas further north in Morocco (Neumaier et al., 2016), iii) significant changes in the supra-evaporite thickness, and/or vi) different lithosphere structure within the basin.

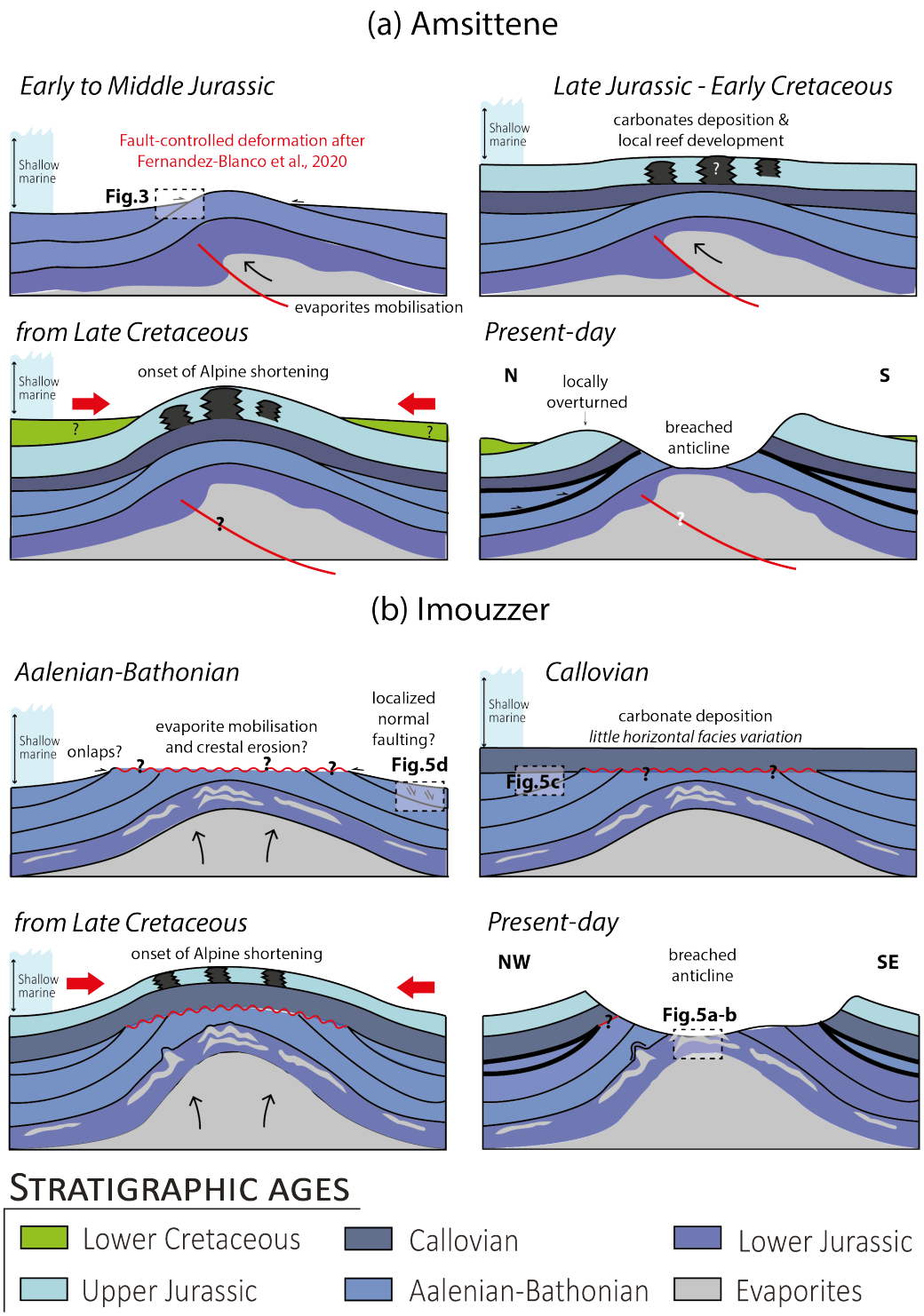

Figure 10 | Conceptual model for the evolution of the a) Amsittène and b) Imouzzer anticlines since the Jurassic. Note that 1) Triassic evaporite presence in the Imouzzer anticline is inferred, 2) this inferred Triassic evaporite was mobile during the Lower and Middle Jurassic, and would either stop before the Callovian or the influx of siliciclatic of the Ameskhoud Fm was so important that it covered completely its topographic expression, and 3) Toarcian evaporites in the Imouzzer anticline were heavily deformed during the initial fold growth.

6.2. Relations with source-to-sink systems

Sediment transport, channel feeder system location and depocenter location (**Fig. 11a**) are likely influenced by the surficial expression of syn-depositional folding and generation of paleo-topography in the EAB. Potential source-to-sink systems in the EAB are illustrated in **figures 12** and **13**, assuming that i) evaporite-cored anticlines were acting as siliciclastic flux barriers, ii) the EAB was characterised by an overall carbonate ramp topography, and iii) the few control points available for some time intervals are sufficient to draw tentative source-to-sink system (e.g., **Fig. 12d** and **e**). **Figures 12** and **13** are similar in nature and differ only for the scale at which they were constructed and for the illustrated periods (exploration well data used in **figure 13** are presented in table 4).

Kilometre-scale erosional exhumation occurs in the Meseta and High Atlas during Middle Jurassic to Early Cretaceous and in the Anti-Atlas during Triassic to Middle Jurassic and Late Cretaceous (**Fig. 11b**; based on a regional synthesis of low-temperature and thermochronology and time-temperature modelling studies; Charton et al., 2018; 2020). Sediment transport with a persistent westward paleo-flow direction in Early Jurassic (e.g., Domenech et al., 2018), Middle and Late Jurassic (Ambroggi, 1963; Stets, 1992), and Cretaceous (Essafraoui et al., 2015; Luber, 2017) was controlled by temporary sinks that developed in the EAB.

In the Central High Atlas, Lower and Middle Jurassic diapirism has been extensively studied (**Fig. 11**; Verges et al., 2017; Teixell et al., 2017; Moragas et al., 2018), where the structures observed show a strong influence of the diapirism on the sedimentation in the corresponding mini-basins. Compared to this area, the diapirism impact on the sedimentation in the EAB is restricted and imply more subtle salt movements during this period.

In the onshore EAB, the end of the Middle Jurassic (Bathonian-Callovian) seems to have recorded the first important halokinetics movements. This is observable in the Imouzzer anticline (**Fig. 10b**), with the angles between the Middle Jurassic carbonate layers (**Fig. 5c**); and in the Amsttene Anticline (**Fig. 10a**), with the onlap structures observed in the north of the anticline. Evidence of halokinetics movements during the Upper Jurassic and Lower cretaceous are harder to identify or disprove due to the constant erosion of these units along the anticline flanks onshore the EAB.

Middle Jurassic-Early Cretaceous evaporite mobility (**Fig. 11**), marked by thickness variations in the up to 10 km wide mini-basins, suggests deep-water sinks may have forced differential loading, thus driving evaporite mobility (**Fig. 13**). Most eroded material was transported over the rifted margin, south into the offshore EAB (Agadir segment; Pichel et al., 2019), where turbiditic deep-water facies were deposited in the Middle Jurassic and Early Cretaceous (**Figs. 13b** and **13c**). The Early Cretaceous fluvial systems that sourced detritus and lead to a sedimentary succession of c. 7 km atop the Triassic evaporite (Pichel et al., 2019) are preserved and exposed in the onshore EAB (Luber, 2017; Luber et al., 2019).

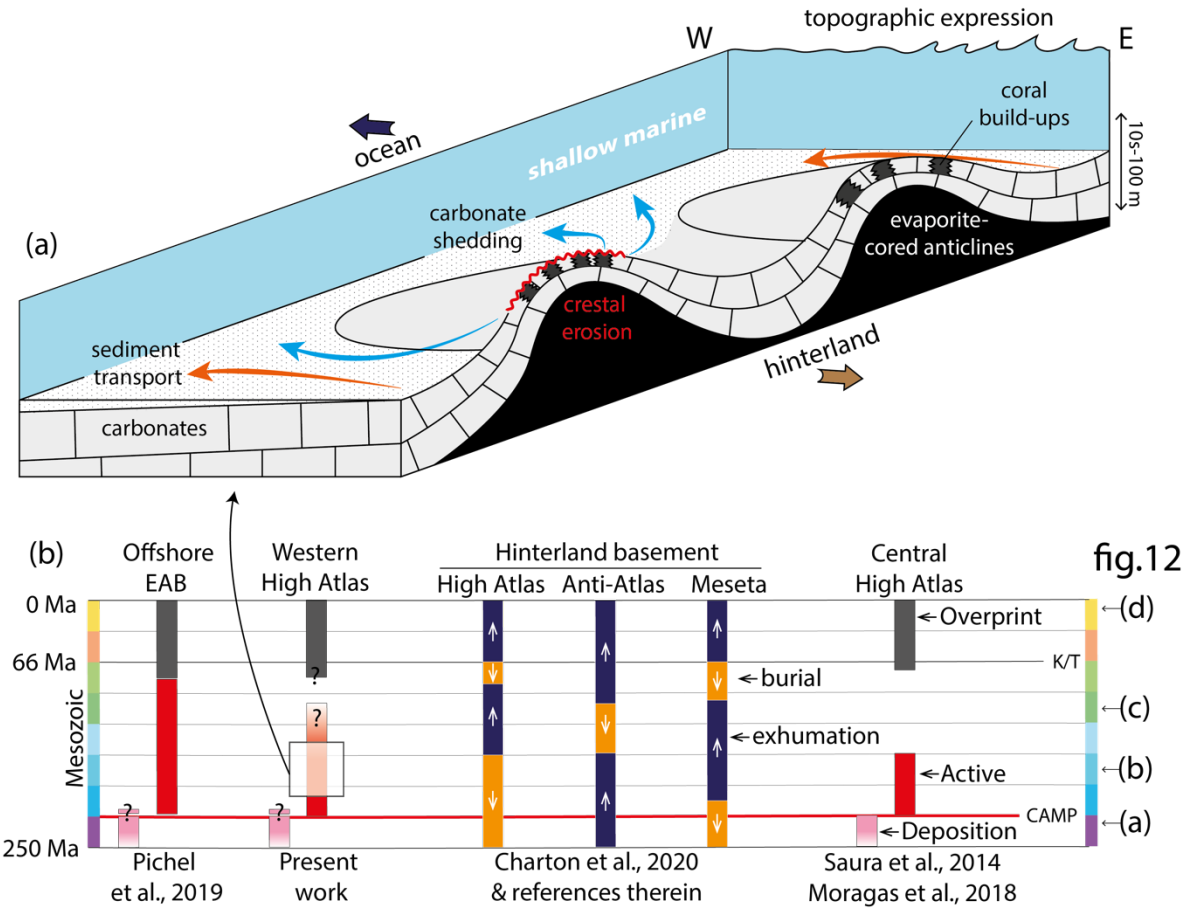

Figure 11 | a) Highly idealized channelization of sediment transport in a shallow marine mixed siliciclastic and carbonate environment due to fold growth and b) timing of evaporite mobilisation and exhumation in surrounding massifs (see references therein).

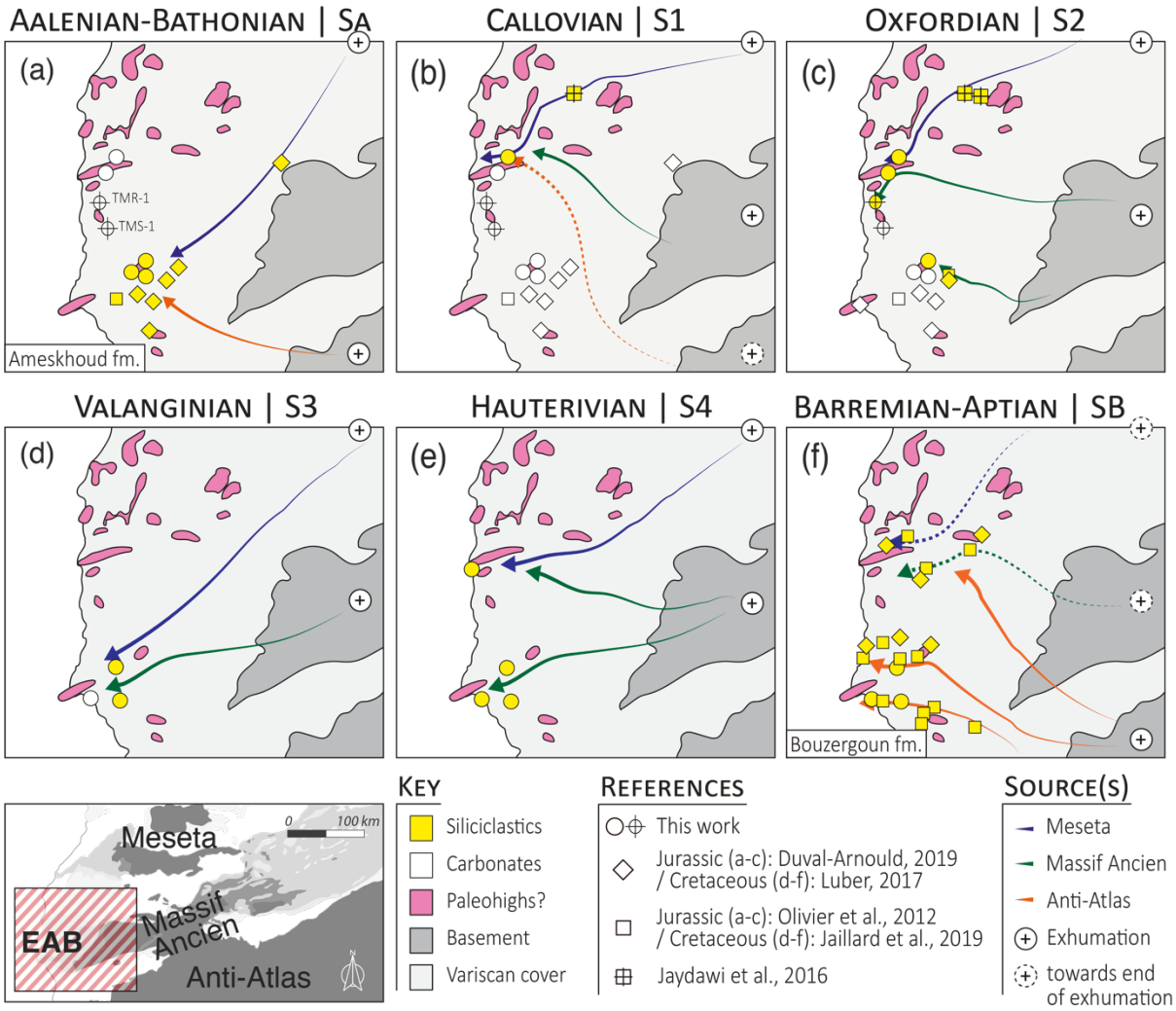

Figure 12 | Tentative reconstruction of Jurassic / Cretaceous source-to-sink systems for identified siliciclastic influx (**Figs. 8 and 9**), ultimately dependent on i) the active sedimentary source at each time and ii) IF each evaporite-cored anticline was indeed forming a paleo-high (see text). Six siliciclastic influx are recognized in the area: a) during the Aalenian-Bathonian ("Sa" for Ameskhoud Fm), b) in the Callovian ("s1"), c) in the Oxfordian ("S2"), d) in the Valanginian (S3), e) in the Hauterivian (S4), and f) in the Late Barremian – Early Aptian ("Sb" for Bouzergoun Fm).

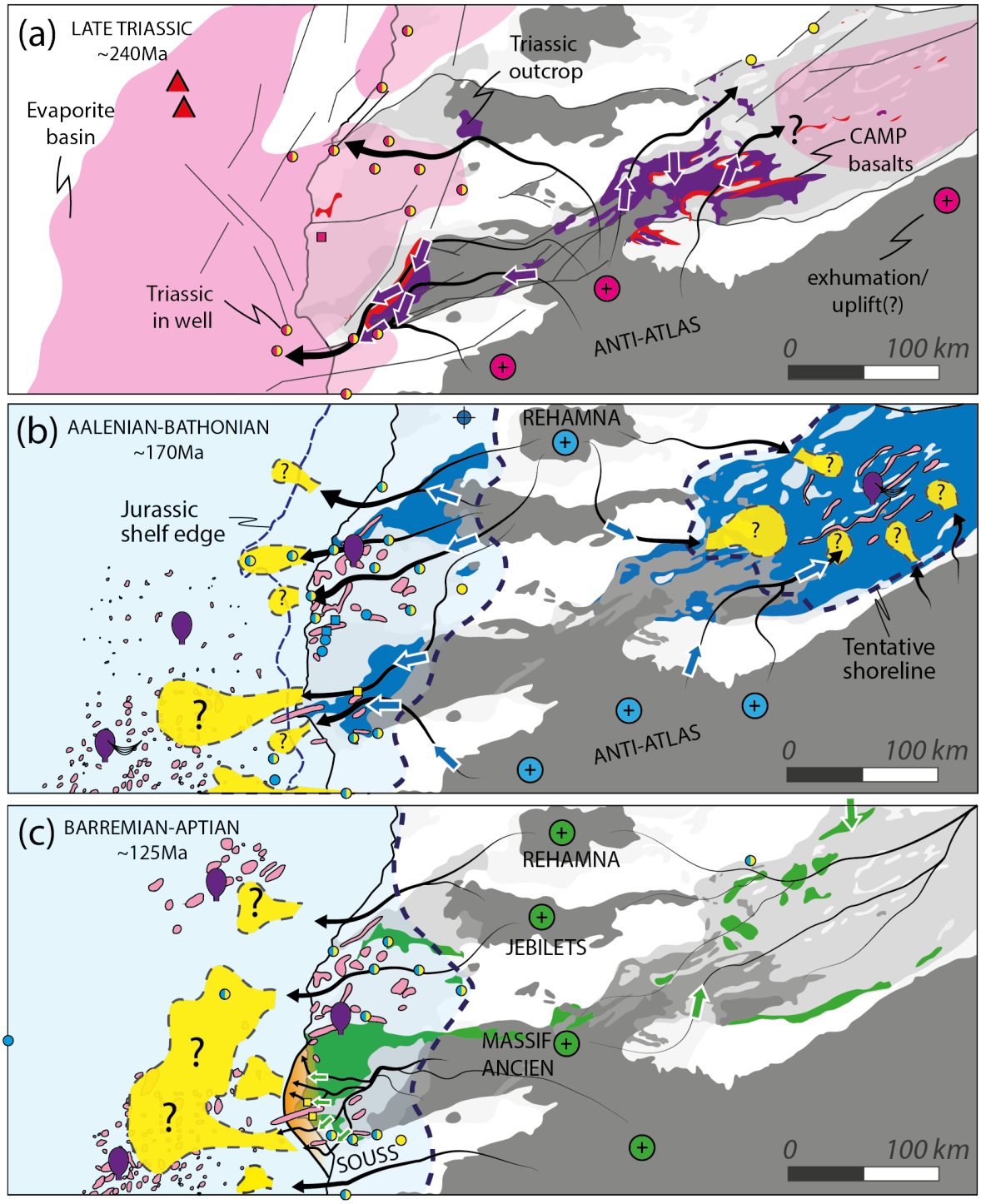

Figure 13 (part 1; see legends in part 2) | Tentative paleo-reconstructions of the EAB and surrounding massifs (made from the compilations of paleogeography, depositional environment, and structural maps; see references below) during four selected times (**Fig. 11b**). Exhumation, presence in subsurface, and tentative shoreline after Charton et al. (2020). Evaporite structures outlined in the offshore of the EAB and High Atlas after Michard et al. (2008), Hafid et al. (2008), and Moragas et al. (2017). Timing of evaporite mobilisation after

figure 11b and references therein. a) Late Triassic map. Evaporite basin outlines after Pichel et al. (2019) and Tari et al. (2012), paleocurrents after Brown (1980), Courel et al. (2003), and Mader (2005), and paleo-reconstruction after Domenech et al. (2018); b) Middle Jurassic map. Tentative shoreline after Charton (2018), paleocurrents after Stets (1992), and paleo-reconstruction, including deep sea fan location, after Nemcok et al. (2005), Lancelot and Winterer (1980) and Tari et al. (2012). c) Barremian-Aptian map. Tentative shoreline after Charton (2018), paleocurrents after Luber (2017), Cavallina et al. (2018), Haddoumi et al. (2019), and paleo-reconstruction, including deep sea fan location, after ONHYM (internal document, 2004), Nemcok et al. (2005) and Tari et al. (2013).

Basin	Well code	Approximated location		U.Triassic			M. Jurassic			Barr.-Aptian		
		Lat. [decº]	Long. [decº]	C.C.	F.C.	EV.	C.C.	F.C.	LMST	C.C.	F.C.	LMST
Deep offshore	DSDP-415	31.0	-11.6	-	-	-	-	-	-	0	0	1
EAB Offshore	CS-1	31.3	-10.2	-	-	-	-	-	-	0	1	1
	ESR-1X	31.6	-10.2	-	-	-	1	-	1	-	-	-
	ESW-1bis	31.5	-9.9	1	1	1	1	1	1	-	-	-
EAB Onshore	TMR-1	30.9	-9.7	0	1	1	0	0	1	-	-	-
	TMS-1	31.0	-9.7	0	0	1	0	0	1	-	-	-
	TAT-1	31.3	-9.7	-	-	-	1	1	1	-	-	-
	TAB-1	31.3	-9.8	-	-	-	0	1	1	-	-	-
	ZEL-1	31.3	-9.3	-	-	-	0	0	1	1	1	1
	BZ-1	31.3	-9.1	1	1	1	1	1	1	-	-	-
	ESS-1	31.6	-9.7	0	1	1	0	1	1	1	1	1
	DIR-1	31.6	-9.0	0	1	1	1	1	1	1	1	1
	DKS-1	31.5	-9.2	1	1	1	1	1	0	1	1	1
	MKL-109	31.4	-9.4	0	1	1	0	1	1	1	1	1
	RJK-1	31.3	-9.0	0	1	1	1	0	0	1	1	1
Souss Offshore	BTS-1	30.5	-10.0	1	1	1	-	-	-	-	-	-
	MCA-1	30.4	-9.9	1	1	1	0	1	1	-	-	-
	AGM-1a	30.2	-9.9	-	-	-	0	0	1	-	-	-
Souss Offshore	LA-1	30.5	-9.6	-	-	-	-	-	-	1	1	1
	TGA-2	30.4	-9.5	0	1	1	1	1	0	0	1	1
	EGA-1	30.5	-9.3	1	1	1	1	1	1	1	1	1
	EGA-2	30.4	-9.3	-	-	-	-	-	-	0	1	0
	HB-1	30.2	-9.5	1	1	1	1	1	1	1	1	1
Doukkala	DOT-1	32.2	-8.9	1	1	1	-	-	-	-	-	-
	MAC-1	31.9	-9.4	0	1	1	0	1	1	-	-	-
Settat	TAN-101	32.1	-7.2	0	1	0	-	-	-	0	1	1
	DRZ-1	32.3	-6.8	1	1	0	-	-	-	-	-	-

Table 4 | Curated well data used in the construction of figure 13 (part 1). CC: Coarse clastics. FC: Fine clastics. EV: Evaporites. LMST: limestones/marls/dolomites. '1': the lithology was recorded in the initial well report. '0': the lithology was not recorded. '-': the interval in this well i) was not traversed, ii) was not deposited/eroded, or iii) is undifferentiated.

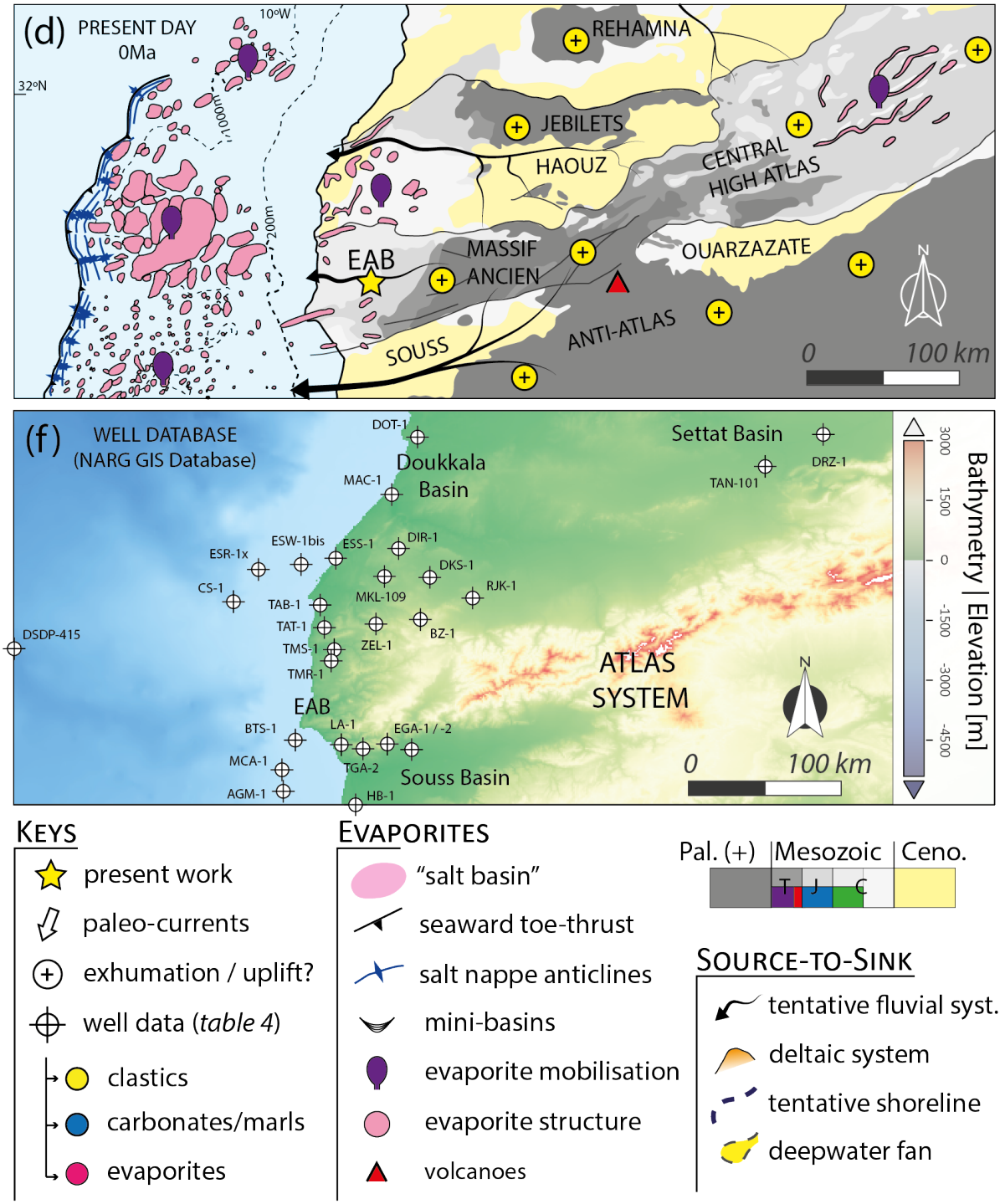

Figure 13 (part 2) | d) Present-day situation. f) Exploration well database, used in the construction of (a), (b) and (c), extracted from the North Africa Research Group (NARG) GIS Database. DEM data: GEBCO_2014_1D.

7. Conclusions

This study sheds new light onto the controversial question about whether evaporite-cored folds in the EAB are shaped by Mesozoic evaporite mobilisation or Cenozoic compressional forces. The results show that anticline growth was already active during the Early to Middle Jurassic and, before the Atlasic orogeny, and therefore likely due to evaporite mobilisation. Mobilisation of Triassic evaporites layers was most likely initiated by Jurassic exhumation in the hinterland, developing a topographic gradient, and associated differential subsidence in the EAB onshore and offshore (e.g., Ameskhoud and Bouzergoun Fms for which depocenters were dependant on the sediment entry point(s)), causing a hydraulic head gradient that led to lateral evaporite flow).

The observed E-W folding is interpreted to be the results of a gravitational gradient caused by the Jurassic uplift of the Anti-Atlas to the south of the basin. In the Berriasian-Aptian, the Cap Rhir N/S trending paleohigh (depicted in Luber, 2017) could be linked to uplift in the High Atlas massifs to the east. No supporting evidence can be found for the proposed regional shortening in the Jurassic, postulated in previous studies.

As a consequence of early fold growth, the syn-sedimentary structures controlled sediment discharge pathways, and the route of fluvial systems coming from the exhumed Variscan massifs in the hinterland, being shed towards the offshore basin. We postulate that the location of depocenters that may contain deep-water fan sandstones of Jurassic to Early Cretaceous age are in part dependent on the location of the fluvial entry points along the coastal margin, that were controlled by the evaporite-cored anticlines in the EAB that diverted paleoflows.

References

Adams, A.E., 1979. Sedimentary environments and palaeogeography of the Western High Atlas, Morocco, during the Middle and Late Jurassic. Palaeogeography, Palaeoclimatology, Palaeoecology, **28**, pp.185-196.

Adams, A.E., Ager D.V., Harding, A.G., 1980. Géologie de la région d'Imouzzer des Ida-ou-Tanane (Haut Atlas occidental), Notes du Service géologique du Maroc, **41**, p.57

Ager, D.V., 1974. The western High Atlas of Morocco and their significance in the history of the North Atlantic. Proceedings of the Geologists' Association, **85**(1), pp.23.

Alves, T.M., Gawthorpe, R.L., Hunt, D.W. and Monteiro, J.H., 2002. Jurassic tectono-sedimentary evolution of the Northern Lusitanian Basin (offshore Portugal). Marine and Petroleum Geology, **19**(6), pp.727-754.

Alves, T.M., Manuppella, G., Gawthorpe, R.L., Hunt, D.W. and Monteiro, J.H., 2003. The depositional evolution of diapir-and fault-bounded rift basins: examples from the Lusitanian Basin of West Iberia. Sedimentary Geology, **162**(3-4), pp.273-303.

Ambroggi, R., 1963. Etude géologique du versant méridional du Haut Atlas occidental et de la plaine du Souss. Editions du Service géologique du Maroc.

Bertotti, G. and Gouiza, M., 2012. Post-rift vertical movements and horizontal deformations in the eastern margin of the Central Atlantic: Middle Jurassic to Early Cretaceous evolution of Morocco. International Journal of Earth Sciences, **101**, pp.2151-2165.

Bouaouda, M.S., (2004). Le bassin Atlantique marocain d'El Jadida-Agadir : stratigraphie, paléogéographie, géodynamique et microbiostratigraphie de la série Lias-Kimméridgien. Thèse Doctorat es-Sciences, Université Mohamed V-Agdal, Rabat., pp. 335.

Brown, R.H., 1980. Triassic rocks of Argana Valley, southern Morocco, and their regional structural implications. AAPG Bulletin, **64**, pp.988-1003.

Bryers, in progress. Ongoing doctoral work. Published work: Bryers, O., Bulot., L., Redfern, J., Casson, M., Ettachfini, M., Masrour, M, Rehakova, D and Jeremiah, J. (2019) Establishing a high resolution integrated stratigraphic framework for the Berriasian to early Barremian of the Morocco Atlantic Margin. PESGB-HGS Africa E&P Conference, October 2019, London.

Cavallina, C., Papini, M., Moratti, G. and Benvenuti, M., 2018. The late Mesozoic evolution of the Central High Atlas domain (Morocco): Evidence from the paleo-drainage record of the Adrar Aglagal syncline. Sedimentary Geology, 376, pp.1-17.

Charton, R., 2018. Phanerozoic Vertical Movements in Morocco. Doctoral dissertation, Delft University of Technology, 165 pp.

Charton, R., Bertotti, G., Arantegui, A. and Bulot, L., 2018. The Sidi Ifni transect across the rifted margin of Morocco (Central Atlantic): Vertical movements constrained by low-temperature thermochronology. Journal of African Earth Sciences, 141, pp.22-32.

Charton, R., Bertotti, G., Duval Arnould, A., Storms, J.E. and Redfern, J., 2020. Low-temperature thermochronology as a control on vertical movements for semi-quantitative source-to-sink analysis: A case study for the Permian to Neogene of Morocco and surroundings. Basin Research, 47p. doi.org/10.1111/bre.12517

Choubert, G., 1957. Carte géologique du Maroc au 1/500.000, feuille Marrakech. Notes et Mémoires du Service géologique du Maroc, 70.

Company, M., Sandoval, J., Tavera, J.M., Aoutem, M., Ettachfini, M., 2008. Barremian ammonite faunas from the western High Atlas, Morocco – biostratigraphy and palaeobiogeography. Cretaceous Research 29, 9–26.

Courel, L., Salem, H.A., Benaouiss, N., Et-Touhami, M., Fekirine, B., Oujidi, M., Soussi, M. and Tourani, A., 2003. Mid-Triassic to Early Liassic clastic/evaporitic deposits over the Maghreb Platform. Palaeogeography, Palaeoclimatology, Palaeoecology, 196, pp.157-176.

Dahlstrom, C. D. A., 1969. Balanced cross sections, Can. J. Earth Sci., 6, p. 743–757.

Davison, I. and Barreto, P., 2020. Deformation and sedimentation processes, and hydrocarbon accumulations on upturned salt diapir flanks in the Lusitanian Basin, Portugal. Petroleum Geoscience, 27(1), petgeo2019-138

Davies, J.H.F.L., Marzoli, A., Bertrand, H., Youbi, N., Ernesto, M. and Schaltegger, U., 2017. End-Triassic mass extinction started by intrusive CAMP activity. Nature communications, 8, pp.1-8.

Domenech, M., 2015. Rift opening and inversion in the Marrakech High Atlas: integrated structural and thermochronologic study: Universitat Autònoma de Barcelona, Ph.D. Thesis, 157 p.

Domènech, M., Stockli, D. and Teixell, A., 2018. Detrital zircon U-Pb provenance and paleogeography of Triassic rift basins in the Marrakech High Atlas: Terra Nova, 30, p. 310-318. doi:10.1111/ter.12340

Du Dresnay, R., 1988. Répartition des dépôts carbonatés du Lias inférieur et moyen le long de la côte atlantique du Maroc: conséquences sur la paléogéographie de l'Atlantique naissant. Journal of African Earth Sciences (and the Middle East), 7(2), pp.385-396.

Duffaud, F., 1960. Contribution à l'étude stratigraphique du bassin secondaire du Haut-Atlas occidental (Sud-Ouest marocain). Bulletin de la Société géologique de France, 7(6), pp.728-734.

Duffaud, F., 1964. Carte géologique du Maroc au 1/100 000, feuille Tamanar. Notes & Mém. Serv. géol. Maroc, 201.

Duffaud, F., Brun, L. and Plauchut, B., 1966. Le bassin du Sud-Ouest marocain. In Reyre D.(édit.): Bassins sédimentaires du littoral africain. Symp. New Delhi, Publ. Assoc. Serv. géol. Afr., Paris, I, pp. 5-26.

Dunham, R. J., 1962. Classification of carbonate rocks according to depositional texture. In Classification of Carbonate Rocks—A Symposium, The American Association of Petroleum Geologists, (ed. Ham, W. E.) pp. 108–121.

Durand-Riard, P., Caumon, G. and Muron, P., 2010. Balanced restoration of geological volumes with relaxed meshing constraints. Computers & Geosciences, 36, pp.441-452.

Duval-Arnould A.,2019. Controls on stratigraphic development of shelf margin carbonates: Jurassic Atlantic margin – Essaouira-Agadir Basin, Western Morocco: PhD Thesis, University of Manchester, 287p.

Ellero, A., Ottria, G., Malusà, M.G. and Ouanaimi, H., 2012. Structural geological analysis of the High Atlas (Morocco): evidences of a transpressional fold-thrust belt. Tectonics-Recent Advances.

Ellero, A., Malusà, M.G., Ottria, G., Ouanaimi, H. and Froitzheim, N., 2020. Transpressional structuring of the High Atlas belt, Morocco. Journal of Structural Geology, p.104021. doi: 10.1016/j.jsg.2020.104021

Elliot, D., 1983. The construction of balanced cross-section. Journal of Structural Geology, 5.

Ellouz, N., Patriat, M., Gaulier, J.-M., Bouatmani, R. and Sabounji, S.,2003. From rifting to Alpine inversion: Mesozoic and Cenozoic subsidence history of some Moroccan basins: Sedimentary Geology, 156, p. 185–212. doi:10.1016/S0037-0738(02.00288-9

Embry, A.F. and Klovan, J.E., 1971. A late Devonian reef tract on northeastern Banks Island, NWT. Bulletin of Canadian petroleum geology, 19(4), pp.730-781.

Essafraoui, B., Ferry, S., Groshény, D., Içame, N., El Aouli, H., Masrour, M., Bulot, L.G., Géraud, Y. and Aoutem, M., 2015. Sequence stratigraphic architecture of marine to fluvial deposits across a passive margin (Cenomanian, Atlantic margin, Morocco, Agadir transect). Carnets de géologie.

Ettachfini, M., 2004. Les ammonites néocomiennes dans l'Atlas atlantique (Maroc): biostratigraphie, paléontologie, paléobiogeographie et paléoécologie. Strata, Mémoire, **43**, 1–223.

Fernández-Blanco, D., Gouiza, M., Charton, R. J., Kluge, C., Klaver, J., Brautigam, K., and Bertotti, G., 2020. Anticline growth by shortening during crustal exhumation of the Moroccan Atlantic margin. Journal of Structural Geology. doi:10.31223/osf.io/u3g5j

Ferry, S., Masrour, M and Grosheny, D., 2007. Le Crétacé de la marge atlantique marocaine

(région d'Agadir). Excursion du Groupe Français du Crétacé, Série "Excursion", 75 p.

Folk, R.L., 1980. Petrology of Sedimentary Rocks. Hemphill Publishing Co., Austin, Texas, 182 p.

Frizon de Lamotte, D., Leturmy, P., Missenard, Y., Khomsi, S., Ruiz, G., Saddiqi, O., Guillocheau, F. and Michard, A., 2009. Mesozoic and Cenozoic vertical movements in the Atlas system (Algeria, Morocco, Tunisia): An overview. Tectonophysics, **475**, p. 9–28. doi:10.1016/j.tecto.2008.10.024

Frizon de Lamotte, D., Saint Bezar, B., Bracène, R. and Mercier, E., 2000. The two main steps of the Atlas building and geodynamics of the western Mediterranean. Tectonics, 19(4), pp.740-761. Doi: 10.1029/2000TC900003

Frizon de Lamotte, D., Tavakoli-Shirazi, S., Leturmy, P., Averbuch, O., Mouchot, N., Raulin, C., Leparmentier, F., Blanpied, C. and Ringenbach, J.C., 2013. Evidence for Late Devonian vertical movements and extensional deformation in northern Africa and Arabia: integration in the geodynamics of the Devonian world. Tectonics, **32**(2), pp.107-122.

Frizon de Lamotte, D., Zizi, M., Missenard, Y., Hafid, M., El Azzouzi, M., Maury, R.C., Charrière, A., Taki, Z., Benammi, M. and Michard, A., 2008. The atlas system. In Michard et al., 2008. Continental evolution: the geology of Morocco (pp. 133-202). Springer, Berlin, Heidelberg.

Ghorbal, B., 2009. Mesozoic to Quaternary thermo-tectonic evolution of Morocco (NW Africa.: Vrije Universiteit Amsterdam, Ph.D. Thesis, 226 p.

Ghorbal, B., Bertotti, G., Foeken, J. and Andriessen, P.,2008. Unexpected Jurassic to Neogene vertical movements in 'stable' parts of NW Africa revealed by low temperature geochronology: Terra Nova, 20, p. 355–363. doi:10.1111/j.1365-3121.2008.00828.x

Gouiza, M., Charton, R., Bertotti, G., Andriessen, P. and Storms, J.E.A., 2017. Post-Variscan evolution of the Anti-Atlas belt of Morocco constrained from low-temperature geochronology. International Journal of Earth Sciences, 106, pp.593-616.

Haddoumi, H., Charrière, A., Feist, M., Baidder, L., Ferrière, J., Karim, M., Ettachfini, E.M., Mamoun, S.M., Chennouf, R., Rachdi, A. and Adardor, S., 2019. A Barremian-? Aptian Tethyan precursor of the Cretaceous marine flooding of Morocco: Evidence from the red-bed series within the "Marginal Folds" of the eastern High Atlas. Cretaceous Research, 95, pp.37-60.

Hafid, M., 2000. Triassic–early Liassic extensional systems and their Tertiary inversion, Essaouira Basin (Morocco). Marine and Petroleum Geology, 17, pp.409-429.

Hafid, M., Salem, A.A. and Bally, A.W., 2000. The western termination of the Jebilet–high Atlas system (offshore Essaouira Basin, Morocco). Marine and Petroleum Geology, 17, pp.431-443.

Hafid, M., Tari, G., Bouhadioui, D., El Moussaid, I., Echarfaoui, H., Salem, A.A., Nahim, M. and Dakki, M., 2008. Atlantic basins. In Michard et al., 2008, Continental evolution: The geology of Morocco, (pp. 303-329). Springer, Berlin, Heidelberg.

Hafid, M., Zizi, M., Bally, A.W. and Ait Salem, A.,2006. Structural styles of the western onshore and offshore termination of the High Atlas, Morocco. Comptes Rendus Geoscience, 338, p. 50–64. doi:10.1016/j.crte.2005.10.007

Hoffmann, E. and Winde, F., 2010. Generating high-resolution digital elevation models for wetland research using Google EarthTM imagery: an example from South Africa. Water SA, 36, pp.53-68.

Hollard, H., Choubert, G., Bronner, G., Marchand, J. and Sougy, J., 1985. Carte géologique du Maroc, scale 1: 1,000,000. Serv. Carte géol. Maroc, 260(2).

Hudec, M.R. and Jackson, M.P., 2007. Terra infirma: Understanding evaporite tectonics. Earth-Science Reviews, 82, pp.1-28.

Jaidi, S.E.M., Bencheqroun, A., Diouri, M. and Ennadifi, Y., 1970. Carte Géologique de l'Anti-Atlas central et de la zone synclinale de Ouarzazate 1:200 000, Feuilles Ouarzazate, Alougoum et Telouet Sud. Not. Mém. Serv. Géol. Maroc, 138.

Jaydawi, S., Hssaida, T., Benbouziane, A., Mouflih, M. and Chakor Alami, A., 2016. Datation par les kystes de dinoflagellés des formations jurassiques (Callovien–Kimméridgien) du bassin d'Essaouira (Marge atlantique marocaine). Bulletin de l'Institut Scientifique, Rabat. Section Sciences de la Terre, 38, pp.127-148.

Knight, K.B., Nomade, S., Renne, P.R., Marzoli, A., Bertrand, H. and Youbi, N., 2004. The Central Atlantic Magmatic Province at the Triassic–Jurassic boundary: paleomagnetic and 40Ar/39Ar evidence from Morocco for brief, episodic volcanism. Earth and Planetary Science Letters, 228(1-2), pp.143-160.

Labails, C., Olivet, J.L., Aslanian, D. and Roest, W.R., 2010. An alternative early opening scenario for the Central Atlantic Ocean. Earth and Planetary Science Letters, 297(3-4), pp.355-368.

Lancelot, Y. and Winterer, E.L., 1980. Evolution of the Moroccan oceanic basin and adjacent continental margin—a synthesis. Initial Reports of the Deep-Sea drilling project, 50, pp.801-821.

Luber, T., 2017. Integrated Analysis of Lower Cretaceous Stratigraphy and depositional systems: The Essaouira-Agadir basin of Morocco: University of Manchester, Ph.D. Thesis, 257 p.

Luber, T.L., Bulot, L.G., Redfern, J., Frau, C., Arantegui, A., Masrour, M., 2017. A revised ammonoid biostratigraphy for the Aptian of NW Africa: Essaouira-Agadir Basin, Morocco. Cretaceous Research, 79, 12–34.

Luber, T.L., Bulot, L.G., Redfern, J., Nahim, M., Jeremiah, J., Simmons, M., Bodin, S., Frau, C., Bidgood, M. and Masrour, M., 2019. A revised chronostratigraphic framework for the Aptian

of the Essaouira-Agadir Basin, a candidate type section for the NW African Atlantic Margin. Cretaceous Research, **93**, pp.292-317.

Mader, N.K., 2005. Sedimentology and sediment distribution of Upper Triassic fluvio-aeolian reservoirs on a regional scale (Central Algeria, SW Morocco, NE Canada): an integrated approach unravelling the influence of climate versus tectonics on reservoir architecture (Doctoral dissertation, The University of Manchester (United Kingdom)).

Mader, N.K. and Redfern, J., 2011. A sedimentological model for the continental Upper Triassic Tadrart Ouadou Sandstone Member: recording an interplay of climate and tectonics (Argana Valley; South-west Morocco). Sedimentology, **58**(5), pp.1247-1282.

Mader, N.K., Redfern, J. and El Ouataoui, M., 2017. Sedimentology of the Essaouira Basin (Meskala Field) in context of regional sediment distribution patterns during upper Triassic pluvial events. Journal of African Earth Sciences, **130**, pp.293-318.

Martin-Garin, B., Lathuilière, B., Geister, J., Chellai, E.H. and Huault, V., 2007. Geology, facies model and coral associations of the Late Jurassic reef complex at Cape Ghir (Atlantic High Atlas, Morocco). Comptes Rendus Geoscience, **339**(1), pp.65-74. Doi: 10.1016/j.crte.2006.10.007

Martín-Martín, J.D., Vergés, J., Saura, E., Moragas, M., Messager, G., Baqués, V., Razin, P., Grélaud, C., Malaval, M., Joussiaume, R. and Casciello, E., 2017. Diapiric growth within an Early Jurassic rift basin: The Tazoult salt wall (central High Atlas, Morocco). Tectonics, **36**(1), pp.2-32. Doi: 10.1002/2016TC004300

Masrour, M., 2004. The echinoid faunas of the Lower Cretaceous of the Atlantic High Atlas region (Morocco); systematic revision and biostratigraphical results. Geobios, **37**, 595–617.

Michard, A., Saddiqi, O., Chalouan, A. and Frizon de Lamotte, D., 2008. Continental Evolution: The Geology of Morocco: Springer-Verlag, Berlin Heidelberg, 116, 424 p.

Michard, A., Soulaimani, A., Hoepffner, C., Ouanaimi, H., Baidder, L., Rjimati, E.C. and Saddiqi, O., 2010. The south-western branch of the Variscan Belt: evidence from Morocco. Tectonophysics, 492(1-4), pp.1-24.

Mitra, S. and Namson, J.S., 1989. Equal-area balancing. American Journal of Science, **289**, pp.563-599.

Moragas, M., Vergés, J., Saura, E., Martín-Martín, J., Messager, G., Merino-Tomé, Ó., Suárez-Ruiz, I., Razin, P., Grélaud, C., Malaval, M., Joussiaume, R. and Hunt, D. W., 2018. Jurassic rifting to post-rift subsidence analysis in the Central High Atlas and its relation to evaporite diapirism: Basin Research, 30, 336-362. doi:10.1111/bre.12223

Moragas, M., Vergés, J., Nalpas, T., Saura, E., Martín-Martín, J.D., Messager, G. and Hunt, D.W., 2017. The impact of syn-and post-extension prograding sedimentation on the development of evaporite-related rift basins and their inversion: Clues from analogue modelling. Marine and Petroleum Geology, **88**, pp.985-1003.

Moretti, I., 2008. Working in complex areas: New restoration workflow based on quality control, 2D and 3D restorations. Marine and Petroleum Geology, **25**, pp.205-218.

Nemčok, M., Stuart, C., Segall, M.P. and Allen, R.B.,2005. Structural development of southern Morocco: Interaction of tectonics and deposition: Annual Bob F. Perkins Research Conference, 25, Houston p. 151–202.

Neumaier, M., Back, S., Littke, R., Kukla, P.A., Schnabel, M. and Reichert, C., 2016. Late Cretaceous to Cenozoic geodynamic evolution of the Atlantic margin offshore Essaouira (Morocco). Basin Research, 28(5), pp.712-730.

Olivier, N., Martin-Garin, B., Colombie, C., Cornee, J.J., Giraud, F., Schnyder, J., Kabbachi, B. and Ezaidi, K., 2012. Ecological succession evidence in an Upper Jurassic coral reef system (Izwarn section, High Atlas, Morocco). Geobios, 45(6), pp.555-572.

Ouajhain, B., Daoudi, L., Laduron, D., Rocha, F. and Jean, N.A.U.D., 2011. Jurassic clay mineral sedimentation control factors in the Essaouira Basin (Western High Atlas, Morocco). Geologica belgica.

Perez, N.D., Teixell, A., Gómez-Gras, D. and Stockli, D.F., 2019. Reconstructing extensional basin architecture and provenance in the Marrakech High Atlas of Morocco: Implications for rift basins and inversion tectonics. Tectonics, 38(5), pp.1584-1608.

Peybernès, B., Bouaouda, M.S., Almeras, Y., RUGET, C. and Cugny, P., 1987. Stratigraphy of THE LIAS/DOGGER deposits from the Essaouira Coastal Basin (Morocco) before and during the beginning of Oceanic accretion in the Central Atlantic – Comparisons with the Agadir Basin. Comptes Rendus de l'Academie des Sciences. Série II, **305**(18), pp.1449-1455.

Pichel, L., 2018. Tectono-stratigraphic evolution associated with evaporite tectonics along Atlantic margins: effects of pre-evaporite relief and regional events (Doctoral dissertation, University of Manchester).

Pichel, L.M., Huuse, M., Redfern, J. and Finch, E., 2019. The influence of base-evaporite relief, rift topography and regional events on evaporite tectonics offshore Morocco. Marine and Petroleum Geology, 103, pp.87-113.

Piqué, A., Le Roy, P. and Amrhar, M., 1998. Transtensive synsedimentary tectonics associated with ocean opening: the Essaouira–Agadir segment of the Moroccan Atlantic margin. Journal of the Geological Society, 155, pp.913-928.

Piqué, A., Soulaimani, A., Laville, E., Amrhar, M., Bouabdelli, M., Hoepffner, C. and Chalouan, A., 2006. Géologie du Maroc: Editions Geode. 287 p.

Piqué, A., Tricart, P., Guiraud, R., Laville, E., Bouaziz, S., Amrhar, M., and Ouali, R.A., 2002. The Mesozoic-Cenozoic atlas belt (North Africa): an overview. Geodinamica Acta, 15, pp. 185–202.

Piqué, A. and Carpenter, M.S., 2001. Geology of northwest Africa. Gebrüder Borntraeger, 29.

Rey, J., Canérot, B., Peybernès, B., Taj-Eddine, K., Rahhali, I., Thieuloy, J.-P., 1986. Le Crétacé inférieur de la région d'Essaouira: données biostratigraphiques et évolutions sédimentaires. Revue de la Faculté des Sciences de Marrakech, Numéro spécial (2), 413-411.

Rey, J., Canérot, J., Peybernès, B., Taj-Eddine, K., Thieuloy, J-P., 1988. Lithostratigraphy, biostratigraphy and sedimentary dynamics of the Lower Cretaceous deposits on the northern side of the western High Atlas (Morocco). Cretaceous Research (9) 141–158.

Richard, J.U. and Ogba, C., 2016. Analysis of Accuracy of Differential Global Positioning System (DGPS) and Google Earth Digital Terrain Model (DTM) Data Using Geographic Information System Techniques. Journal of Geodesy and Geomatics Engineering, 2, pp. 52-61

Roch, E., 1930. Etudes géologiques dans la région méridionale du Maroc Occidental. Notes et Mémoires du Service des Mines et de la Cartes Géologiques Maroc 9, 1–542.

Rojo, L.A. and Escalona, A., 2018. Controls on minibasin infill in the Nordkapp Basin: Evidence of complex Triassic synsedimentary deposition influenced by evaporite tectonics. AAPG Bulletin, 102, pp.1239-1272.

Rusli, N., Majid, M.R. and Din, A.H.M., 2014. Google Earth's derived digital elevation model: A comparative assessment with Aster and SRTM data. In IOP Conference Series: Earth and Environmental Science, IOP Publishing, **18**, p. 012065.

Saddiqi, O., Haimer, El, F.Z., Michard, A., Barbarand, J., Ruiz, G.M.H., Mansour, E.M., Leturmy, P. and de Lamotte, D.F., 2009. Apatite fission-track analyses on basement granites from south-western Meseta, Morocco: Paleogeographic implications and interpretation of AFT age discrepancies. Tectonophysics, 475, p. 29–37. doi:10.1016/j.tecto.2009.01.007

Saura, E., Vergés, J., Martín-Martín, J.D., Messager, G., Moragas, M., Razin, P., Grélaud, C., Joussiaume, R., Malaval, M., Homke, S. and Hunt, D.W., 2014. Syn-to post-rift diapirism and minibasins of the Central High Atlas (Morocco): the changing face of a mountain belt. Journal of the Geological Society, **171**, pp.97-105.

Stets, J., 1992. Mid-Jurassic events in the western high Atlas (Morocco). Geologische Rundschau, **81**, pp.69-84.

Taj-Eddine, K., 1992. Le Jurassique terminal et le Crétacé basal dans l'Atlas atlantique (Maroc): biostratigraphie, sédimentologie, stratigraphie séquentielle et géodynamique. Strata **16**, 1–285.

Tari, G., Jabour, H., Molnar, J., Valasek, D. and Zizi, M., 2012. Deep-water exploration in Atlantic Morocco: Where are the reservoirs? In: Tectonics and Sedimentation: Implications for Petroleum Systems, Dengliang Gao, 2013, doi.org/10.1306/13351560M1003141

Tari, G. and Jabour, H., 2013. Evaporite tectonics along the Atlantic margin of Morocco: In: Mohriak, W.U., Danforth, A., Post, P.J., Brown, D.E., Gabor C. Tari, Nemčok, M. and Sinha, S.T., 2020: Conjugate divergent margins: an introduction, Geological Society, London, Special Publications, **369**, p. 337–353. doi:10.1144/SP369.23

Teixell, A., Arboleya, M.-L., Julivert, M. and Charroud, M., 2003. Tectonic shortening and topography in the central High Atlas (Morocco). Tectonics, **22**, TC1051. doi:10.1029/2002TC001460

Teixell, A., Barnolas, A., Rosales, I. and Arboleya, M.L., 2017. Structural and facies architecture of a diapir-related carbonate minibasin (lower and middle Jurassic, High Atlas, Morocco). Marine and Petroleum Geology, **81**, pp.334-360.

Venus, J.H., Mountney, N.P. and McCaffrey, W.D., 2015. Syn-sedimentary evaporite diapirism as a control on fluvial-system evolution: an example from the proximal Permian Cutler Group, SE Utah, USA. Basin Research, **27**, pp.152-182.

Vergés, J., Moragas, M. J.D. Martín-Martín, J.D., Saura, E., Razin, P., Grélaud, C., Malaval, M., Joussiaume, R., Messager, G., Sharp, I., and Hunt, D.W., 2017. Salt tectonics in the Atlas Mountains of Morocco. In: J.I. Soto, G. Tari, J. Flinch (Eds.), Permo-triassic Salt Provinces of Europe, North Africa and the Atlantic Margins, Tectonics and hydrocarbon potential. Elsevier. doi: 10.1002/2016TC004300

Wentworth, C.K., 1922. A scale of grade class terms for clastic sediments. J. Geol., 30, pp. 377-392

Wippich, M.G.E., 2001. Valanginian (Early Cretaceous) ammonite faunas from the western High Atlas, Morocco, and the recognition of western Mediterranean 'standard' zones. Cretaceous Research, **24**, 357–374.

Zühlke, R., Bouaouda, M.S., Ouajhain, B., Bechstädt, T. and Leinfelder, R., 2004. Quantitative Meso-/Cenozoic development of the eastern central Atlantic continental shelf, western High Atlas, Morocco. Marine and Petroleum Geology, **21**, pp.225-276. Doi: 10.1016/j.marpetgeo.2003.11.014

Acknowledgements

This contribution is partly the result of the second author's M.Sc. Thesis. We are grateful to the North Africa Research Group (NARG) for sponsoring fieldwork. Academic licenses of the TUDelft were used for Move 2D and GoCAD. Tiago Alves (journal editor), Juan Ignacio Soto (reviewer), and an anonymous reviewer are greatly thanked for significantly improving the original manuscript, twice. Finally, we deeply thank ONHYM (Office National des Hydrocarbures et des Mines) for the ongoing years of partnership with the NARG, providing data and field work support to the Ph.D. students of the NARG, extensively exemplified in this work.